Journal of Medicinal Chemistry

pubs.acs.org/jmc

Article

Rhodium(III)−Picolinamide Complexes Act as Anticancer and Antimetastasis Agents via Inducing Apoptosis and Autophagy

Yun-Qiong Gu, Kun Yang, Qi-Yuan Yang, Huan-Qing Li, Mei-Qi Hu, Meng-Xue Ma, Nan-Feng Chen, Yang-Han Liu, Hong Liang,* and Zhen-Feng Chen*

Cite This: J. Med. Chem. 2023, 66, 9592−9606

Read Online

ACCESS | Metrics & More | Article Recommendations | Supporting Information

ABSTRACT: As a continuation of our endeavors in discovering metal-based drugs with cytotoxic and antimetastatic activities, herein, we reported the syntheses of 11 new rhodium(III)−picolinamide complexes and the exploration of their potential anticancer activities. These Rh(III) complexes showed high antiproliferative activity against the tested cancer cell lines in vitro. The mechanism study indicated that **Rh1** ([Rh(**3a**)-$(CH_3CN)Cl_2$]) and **Rh2** ([Rh(**3b**)$(CH_3CN)Cl_2$]) inhibited cell proliferation by multiple modes of action via cell cycle arrest, apoptosis, and autophagy and inhibited cell metastasis via FAK-regulated integrin β1-mediated suppression of EGFR expression. Furthermore, **Rh1** and **Rh2** significantly inhibited bladder cancer growth and breast cancer metastasis in a xenograft model. These rhodium(III) complexes could be developed as potential anticancer agents with antitumor growth and antimetastasis activity.

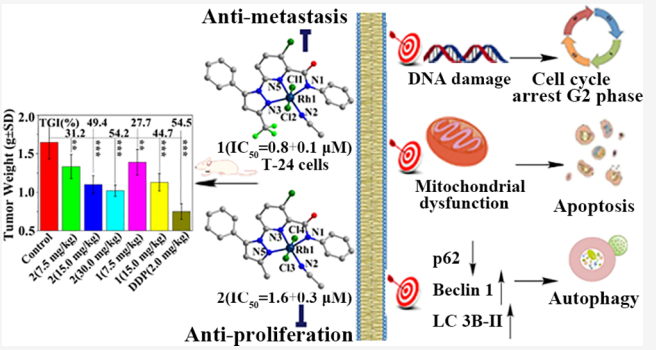

INTRODUCTION

Cancer seriously threatens human health and life, and metastatic spread of cancer cells is the main clinical complication of cancer that causes more than 90% of cancer-related deaths.[1,2] Chemotherapy is still the most common and effective therapeutic method in treating the evolving cancers.[3] Among the chemotherapy drugs, platinum complexes such as oxaliplatin, carboplatin, and cisplatin are widely applied in the treatment of solid tumors. However, their dose toxicity, low selectivity, drug resistance, and low efficacy for metastatic tumors hindered their wider applications.[4] Therefore, the development of new metal complexes that can inhibit both tumor growth and metastasis via multiple modes of action is a promising chemotherapy strategy for cancer.

Metastasis is a multistep continuous process involving a complex series of dynamic events, such as epithelial−mesenchymal transition (EMT), angiogenesis, inflammatory tumor microenvironment initiation, and apoptotic dysfunction.[5] Tumor cells metastasize and spread when EMT occurs in the primary tumor. The early step of EMT is the local infiltration of the surrounding extracellular matrix (ECM) and the stromal cell layer.[6] Cancer cells degrade ECMs by concentrating the enzyme activity of matrix metalloproteinases (MMPs) using special F-actin-rich projections, which allows cancer cells to migrate and invade outside the microenvironment.[7,8] The EGFR signaling pathway and the integrin signaling pathway are involved in regulating many cellular functions.[9] Focal adhesion kinase (FAK) is one of the most significant downstream effector factors that targets cell adhesion to ECM and mediates downstream signal events of ECM integrin conjugation.[10,11] Thus, FAK plays a vital role in cell migration and invasion.[12,13]

Metal complexes are an important class of compounds in anticancer drug development owing to their unique physical, chemical, and structural characteristics and biological activities. Serious side effects of platinum drugs have led to the investigation of other transition-metal complexes,[14] such as ruthenium,[15] rhodium,[16] and palladium[17] complexes. Compared with the typical square-planar Pt(II) complexes, Rh(III) complexes show more structural diversity,[18] high cellular uptake,[19] strong antiproliferative activity,[20] and positive tolerance in normal cells.[21,22] The rhodium(III) centers are traditionally considered inactive, but recent studies have shown that the reactivity to biological targets could be enhanced by coordinating appropriate ligands.[23] These complexes act as inhibitors of proteins or regulators of protein−protein interactions. For example, they are shown to be inhibitors of enzymes,[24] such as the platelet-activating factor (PAF) and thrombin,[23] isomerase,[25] lysine-specific demethylase 5A

Received: February 22, 2023
Published: July 11, 2023

https://doi.org/10.1021/acs.jmedchem.3c00318
J. Med. Chem. 2023, 66, 9592−9606

(KDM5A),[26] and lysine-specific demethylase 1 (LSD1).[27] The unique characteristics of these rhodium complexes, especially their octahedral geometry, allow specific interactions with the appropriate regions of chemical space in protein-binding pockets that are inaccessible to small organic molecules. Rhodium metallo-insertors have high affinity and specific binding to DNA mismatches in vitro, specifically target nuclear DNA, and exhibit cell-selective cytotoxic and antiproliferative activities,[19,28,29] which have attracted our interest in further studying their biological effects.

A substantial number of heterocyclic compounds have been approved for cancer treatment,[30] and the backbones of their structures are often nitrogen heterocycles.[31] Among them, many drugs containing picolinamide or pyrazole have been used in clinical practice to treat cancer (Figure 1).[32,33] The

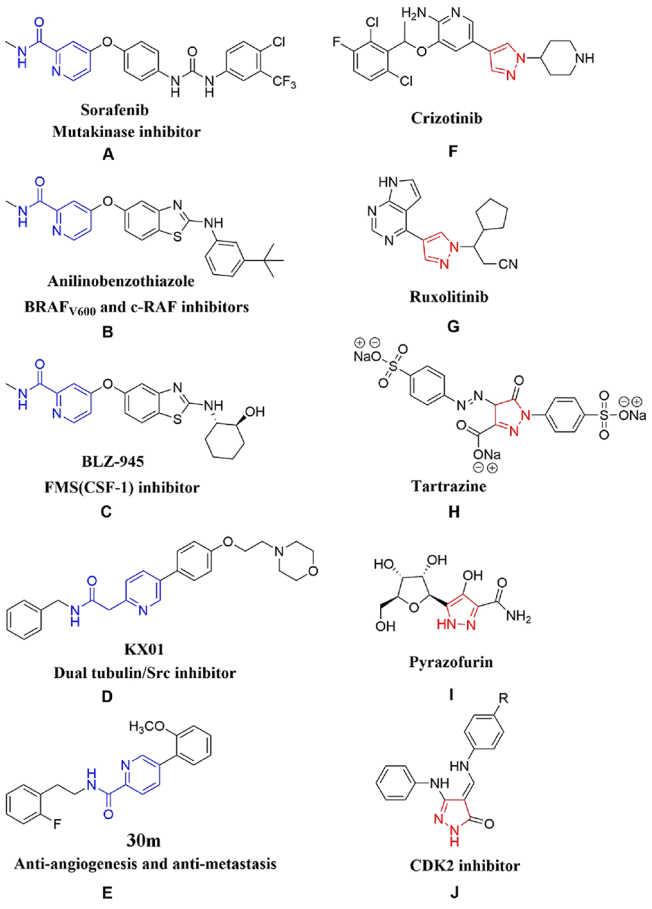

Figure 1. Anticancer agents with picolinamide (**A**–**E**) or pyrazole (**F**–**J**) moiety.

representative anticancer drug sorafenib (Figure 1A), which contains picolinamide structural units, is an inhibitor of several tyrosine kinases (rtk) with potent antitumor and antiangiogenic activities.[34] Many picolinamide derivatives were potent kinase inhibitors, such as 2-anilinobenzothiazole derivatives[35] (BRAFV600E, Figure 1B) for C-raf inhibitors, BLZ-945[36] for FMS inhibitor, Klisyri (KX01, Figure 1D) for the dual microtubulin/Src protein inhibitor,[37] and 30m (Figure 1E) for hypoxia-inducible factor 1 (HIF-1) inhibitor.[38] Meanwhile, pyrazole derivatives occupy a special position in cancer therapy,[39] including crizotinib (Figure 1F), ruxolitinib (Figure 1G), tartrazine (Figure 1H), pyrazofurin (Figure 1I), and 5-anilino-pyrazole analogue I (Figure 1J).[40] In addition, some picolinamide derivatives show high activity in inhibiting tumor cell metastasis.[41,42] The development of new picolinamide and pyrazole compounds with low toxicity and high activity has attracted extensive attention in the field of medicinal chemistry.[33] The pharmacophore conjugation strategy is an effective approach to find new chemical entities with improved biological activity.[32] Using this strategy, we synthesized a series of picolinamide derivatives by conjugating them with pyrazole rings with different substitutions (Scheme 1).

Moreover, we are interested in the development of effective and selective Rh(III) complexes with both antiproliferation and antimetastasis activities, and our group has previously reported a mitochondria-accumulating Rh(III) isoquinoline complexes with different modes of action from Pt(II)-based therapeutics.[43] A series of *N*-(3-bromophenyl)picolinamide rhodium(III) complexes exhibited good in vitro cytotoxicity and selectivity index (SI) value of Rh(III) *trans*-diiodide complexes, which is more than 25 times higher than that of cisplatin.[44] Rhodium half-sandwich complexes containing (N,N)-bound picolinamide ligands showed good potential as anticancer agents.[45] Therefore, the rhodium(III) complexes with these picolinamide derivative ligands were synthesized via N−N−N coordination; the rhodium(III) complexes were characterized, and their activity against tumor growth and metastasis in vitro and in vivo were investigated.

RESULTS AND DISCUSSION

Synthesis and Characterization. The synthesis process of ligands **3a**−**3k** is shown in Scheme 2, and the synthesis of their corresponding rhodium complexes **Rh1**−**Rh11** was carried out following the reported procedure.[46] The complexes **Rh1**−**Rh11** were characterized by HRMS, NMR spectroscopy, elemental analysis, powder X-ray diffraction (Figures S49−S50), and single-crystal X-ray diffraction analysis. The coordination mode of each complex is similar. The central metal atom Rh(III) adopts a distorted octahedral geometry and is bonded to three N atoms from the pyridine ring, pyrazole ring, and amide bond,[47] two chloride ions, and a solvent molecule (methanol for **Rh4** and **Rh6** and acetonitrile for other complexes) (Scheme 3 and Figure 2). ^{1}H NMR data of rhodium complexes showed that hydrogen atoms were detached from the amide bonds of the ligands after the formation of the complexes. The loss of hydrogen and the addition of two chlorine ions make the complex electrically neutral.[48] X-ray powder diffraction results confirmed that the structures of the crystallites of **Rh1** and **Rh2** obtained by batch synthesis are consistent with their single-crystal structures. The

Scheme 1. Structure of Picolinamide Derivatives as Potent Antitumor Agents

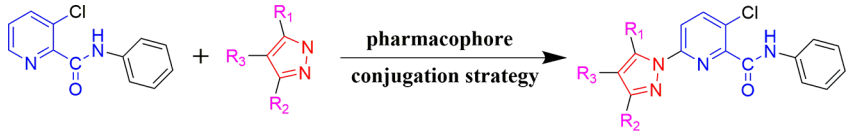

https://doi.org/10.1021/acs.jmedchem.3c00318
J. Med. Chem. 2023, 66, 9592−9606

Scheme 2. Reagents and Conditions: (i) $SOCl_2$, DMF, 85 °C, 3 h; (ii) Aniline, CH_3CN, Triethylamine, 80 °C, 6 h; (iii) Hydrazine Hydrate, Ethanol, 80 °C; and (iv) Ethanol, 90 °C

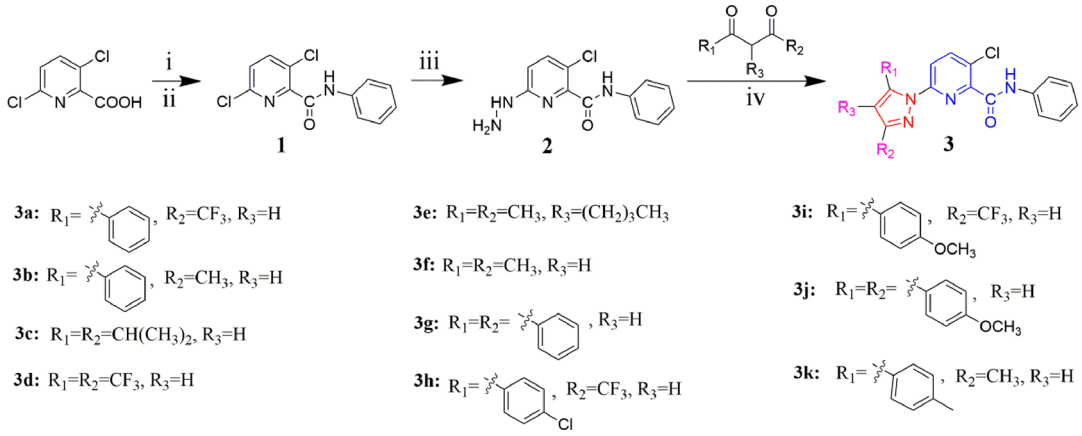

Scheme 3. Synthesis of Complexes Rh1−Rh11; Reagents and Conditions: (i): $RhCl_3·3H_2O$, CH_3CN/CH_3OH (v:v = 4:1, 10 mL), 100 °C, 3 Days

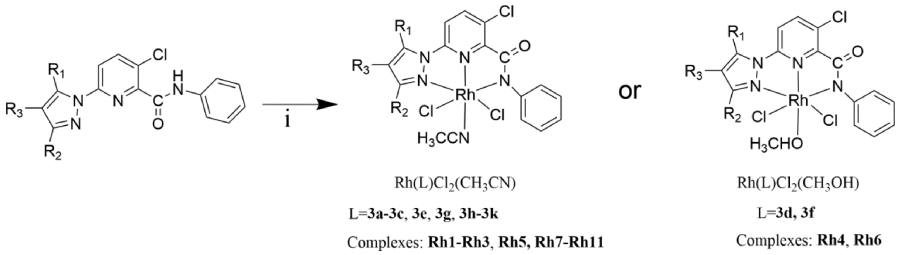

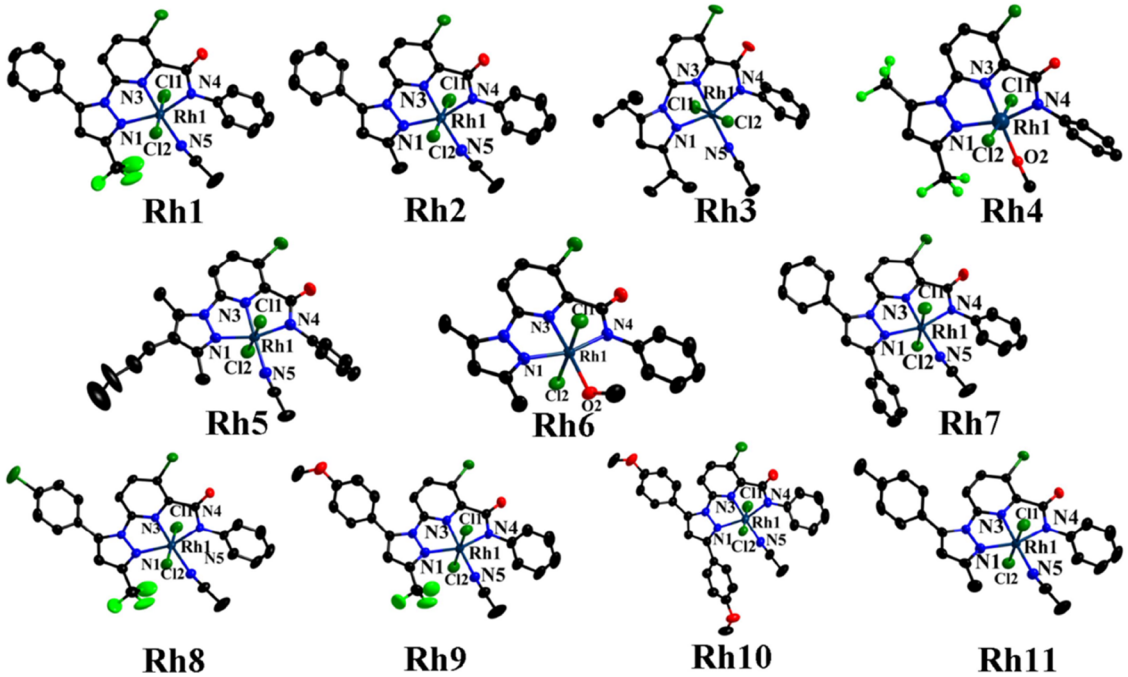

Figure 2. Crystal structures of **Rh1−Rh11** (thermal ellipsoids at 30% probability level; hydrogen atoms are omitted for clarity).

intensity difference of the diffraction peak may be due to the orientation change of the polycrystalline samples. The assignments of each of the H and C resonances of the ligands and rhodium complexes are listed in Tables S1 and S4, and the crystallographic data, selected bond lengths, and angles of **Rh1−Rh11** are presented in Tables S2 and S3.

Stability and Purity of Rh1−Rh11. The stability and purity of **Rh1−Rh11** were detected by the HPLC method in methanol solution (contains no more than 1% DMSO) (Figure S51). The results showed that there were no new peaks that appeared in complexes after 48 h, and the shift of the peaks was almost unchanged, which indicated that **Rh1−Rh11** were stable in solution at least for 48 h at room

https://doi.org/10.1021/acs.jmedchem.3c00318
J. Med. Chem. 2023, 66, 9592−9606

Table 1. IC_{50}[a] (μM) of Rh1−Rh11 for Five Human Cancer Cell Lines[b] Determined by the MTT Method for 48 h

complex	T-24	A549	BEL-7404	HeLa	SK-OV-3	WI38	SF
Rh1	0.8 ± 0.1	1.3 ± 0.4	2.8 ± 0.5	2.5 ± 0.7	3.0 ± 0.7	2.7 ± 0.2	3.4
Rh2	1.6 ± 0.3	7.7 ± 0.3	9.6 ± 0.8	10.0 ± 0.6	13.8 ± 1.4	6.3 ± 0.7	3.9
Rh3	4.4 ± 1.5	10.3 ± 1.2	>20	15.5 ± 1.7	13.9 ± 2.1	15.7 ± 1.0	3.9
Rh4	20.7 ± 0.2	>20	>20	>20	>20	>20	
Rh5	2.0 ± 0.2	5.3 ± 0.2	10.5 ± 1.0	8.3 ± 0.3	10.3 ± 0.5	4.3 ± 1.6	2.2
Rh6	>20	>20	>20	>20	>20	>20	
Rh7	16.9 ± 1.1	>20	>20	16.5 ± 1.7	19.1 ± 1.2	>20	
Rh8	7.2 ± 0.3	9.9 ± 1.2	3.8 ± 0.7	12.1 ± 0.4	7.9 ± 0.4	8.1 ± 0.5	1.1
Rh9	5.9 ± 1.5	6.4 ± 0.6	3.2 ± 0.5	5.7 ± 0.2	2.8 ± 0.7	3.7 ± 0.6	0.6
Rh10	11.6 ± 0.2	18.7 ± 0.9	>20	17.4 ± 0.5	>20	13.3 ± 0.8	1.1
Rh11	2.4 ± 0.3	5.1 ± 0.3	6.5 ± 0.2	4.5 ± 0.3	16.2 ± 0.2	5.3 ± 0.4	2.2
DDP	11.0 ± 0.5	11.4 ± 0.4	34.2 ± 0.7	16.6 ± 0.4	7.9 ± 1.2	5.4 ± 0.9	0.5
$RhCl_3{\cdot}3H_2O$	>40	>40	>40	>40	>40	>40	

[a]IC_{50} values are expressed as mean ± standard deviation of three independent experiments. SF (selectivity factor) = IC_{50}(WI38)/IC_{50}(T-24). [b]T-24 (human bladder cell line), A549 (human non-small-cell lung cancer cells), BEL-7404 (human hepatocellular carcinoma cells), HeLa (human cervical cell line), SK-OV-3 (human ovarian cancer cells), and WI38 (human embryonic lung cell line).

temperature. The purity of all complexes was higher than 95%, as determined by HPLC. The stability of **Rh1**−**Rh11** was also detected by UV−vis spectroscopy (Figure S52). As shown, the absorption peaks near 250 nm showed no changes in peak shape and absorbance, indicating that these complexes remained stable during the experimental time (48 h). The experimental results were consistent with that determined by HPLC.

Lipophilicity Property. The uptake of the complexes by cells is related to their lipophilicity.[49] To determine the lipophilicity of the rhodium complexes, the octanol/water partition coefficients ($\log P_{o/w}$) of the complexes were determined (Figure S53), which suggested the ability of the complexes to cross the cell membranes. Complexes **Rh7**, **Rh8**, and **Rh10** showed negative $\log P_{o/w}$ values, and the other complexes displayed positive $\log P_{o/w}$ values, which indicated that the rhodium complexes are lipophilic except for the hydrophilic **Rh7**, **Rh8**, and **Rh10**. The higher lipophilicity of complexes may promote their cellular uptake and enhance their anticancer activity. Particularly, the lipophilicity of **Rh1**, **Rh2**, **Rh9**, and **Rh11** were greatly improved by introducing a methyl or a trifluoromethyl group on the pyrazole ring of the ligand,[50] whose $\log P_{o/w}$ values were 0.63 ± 0.10, 0.62 ± 0.11, 0.70 ± 0.06, and 0.55 ± 0.06, respectively.

Cytotoxicity of Rhodium Complexes In Vitro. The IC_{50} values of **Rh1**−**Rh11** to five cancer cell lines (BEL-7404, HeLa, A549, T-24, and SK-OV-3) and a normal human embryonic lung cell line WI38 are listed in Table 1. The activity of **Rh1**−**Rh11** against cancer cells (IC_{50} range of 0.8−20 μM) was significantly higher than that of the metal salt $RhCl_3{\cdot}3H_2O$ and the corresponding ligand (both showed IC_{50} greater than 40 μM), indicating that there was a significant synergistic effect after the ligand coordinated with the Rh(III) ion.[50] The rhodium complexes showed a similar trend in IC_{50} values for all tested cancer cells, especially T-24 cells. The order of cytotoxic activity was **Rh1** > **Rh2** > **Rh5** > **Rh11** > **Rh3** > **Rh9** > **Rh8** > **Rh10** > **Rh7** > **Rh4** > **Rh6**. The anticancer activity of the complexes against T-24 was analyzed based on the structure: (1) When R_2=−CF_3, R_3=H and R_1 substituents showed the following order of cytotoxic activity: **Rh1** (−Ph) > **Rh8** (4-Cl-Ph)> **Rh9** (4-OCH_3−Ph) > **Rh4** (−CF_3). (2) When R_2=−CH_3, R_3=H and R_1 substituents showed the following order of cytotoxic activity: **Rh2** (−Ph)> **Rh11** (4-CH_3−Ph)> **Rh6** (−CH_3), and **Rh1** > **Rh2**. (3) To further investigate the effects of substituents R_1 and R_2 on cytotoxicity, we introduced the same substituents at the R_1 and R_2 sites, such as 1-methylethyl (**Rh3**), trifluoromethyl (**Rh4**), methyl (**Rh6**), phenyl (**Rh7**), and *p*-methoxyphenyl (**Rh10**). Complex **Rh3** displayed similar cytotoxic activity as **Rh2**, while the other complexes **Rh4**, **Rh6**, **Rh7**, and **Rh10** revealed poor cytotoxic activity, which may be related to their poor solubility or hydrophilicity, leading to low bioavailability in cells.[51] Notably, when R_1=R_2=−CH_3 and R_3=*n*-butyl (**Rh5**), the cytotoxicity of **Rh5** was significantly enhanced, with an IC_{50} value of 2.0 ± 0.2 μM, at least 10 times higher than that of **Rh6** (R_1=R_2=−CH_3 and R_3=H).

As shown in Table 1, **Rh1** (IC_{50} = 0.8 ± 0.1 μM) and **Rh2** (IC_{50} = 1.6 ± 0.3 μM) were the most cytotoxic to T-24 cells, wherein the cytotoxicity of **Rh1** was 13.5-fold higher than that of cisplatin. Furthermore, the toxicity of **Rh1** and **Rh2** to normal WI38 cells was relatively low, and their selectivity factors for T-24 cells were 3.4 and 3.9, respectively (selectivity factor = IC_{50} (WI38)/IC_{50} (T-24), indicating that the two complexes had moderate selectivity for cancer cells. Therefore, the biological mechanism of the antiproliferative activity of **Rh1** and **Rh2** on T-24 cancer cells was studied.

The time-dependence of **Rh1** and **Rh2** on the cytotoxic activity against T-24 cancer cells was assayed by measuring the IC_{50} values of the complexes after 24 and 48 h treatments (Table 2). It showed that the IC_{50} values of **Rh1** against T-24 cells were 1.7 ± 0.3 and 0.8 ± 0.1 μM after 24 and 48 h, while the values of **Rh2** were 2.5 ± 0.4 and 1.6 ± 0.3 μM, respectively, indicating that the cytotoxic activity of the complexes was treatment time-dependent. For convenience and consistency, the most subsequent mechanism experiments adopted 24 h treatment.

Table 2. IC_{50} (μM) of Rh1 and Rh2 after Different Times of Treatment of T-24 Cells Determined by the MTT Method

complex	IC_{50} after 24 h treatment	IC_{50} after 48 h treatment
Rh1	1.7 ± 0.3	0.8 ± 0.1
Rh2	2.5 ± 0.4	1.6 ± 0.3

Effect on Cell Viability. Cell viability under different treatments was further identified using an image format. Living

https://doi.org/10.1021/acs.jmedchem.3c00318
J. Med. Chem. 2023, 66, 9592−9606

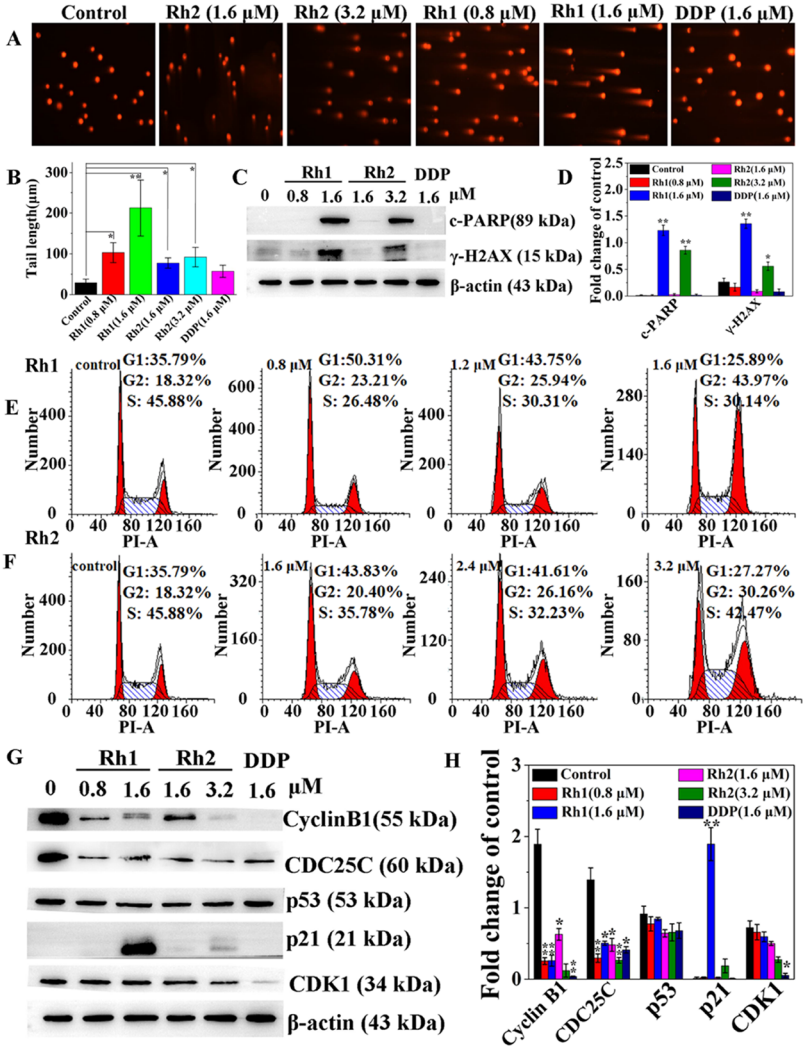

Figure 3. T-24 cancer cells incubated with **Rh1**, **Rh2**, and DDP (24 h). (A) Comet assay performed by fluorescence microscopy with EB staining (with ×400 magnification of the fluorescence microscope). (B) Tail length of the cells in each treated group measured by the comet assay. (C) Changes of *c*-PARP and *γ*-H2AX in cells treated with **Rh1**, **Rh2**, and DDP analyzed by western blot. (D) Histograms displaying the density ratios of *c*-PARP and *γ*-H2AX. Effects of the cell cycle incubated with **Rh1** (0.8, 1.2, and 1.6 μM) (E) and **Rh2** (1.6, 2.4, and 3.2 μM) (F). (G) Western blot assay of the change of the related proteins of the cell cycle. (H) Histograms displaying the density ratios of cell cycle-related proteins.

cells were stained with calcein AM, showing green fluorescence, while dead cells were stained with propidium iodide (PI), showing red fluorescence,[52] to observe the cell viability after different treatments in T-24 cells (Figure S54). With the increasing concentrations of **Rh1** and **Rh2**, the double staining (merge of calcein and PI) showed a significant difference in fluorescence staining between living (green fluorescence) and dead cells (red fluorescence); the number of dead cells marked in red fluorescence increased significantly. The colony formation assays were also used to investigate the antiproliferation activity of the rhodium complexes, which showed that cell viability was significantly inhibited by increasing the dose of **Rh1** and **Rh2** (Figure S55). Especially, when the cells were treated with 0.8 μM **Rh1**, almost no living cells were observed. These results showed that the two complexes could notably inhibit the activity of T-24 cells, which was consistent with the MTT assay results.

Uptake and Distribution. The cell uptake of rhodium complex was closely related to its antitumor activity and mechanisms.[53] The uptake and distribution of **Rh1** and **Rh2** in T-24 cells were detected by the ICP-MS method (Figure S56 and Table S5). After 10 h of incubation with **Rh1** and **Rh2** (8.0 μM), the total rhodium accumulation in the cells was dramatically increased compared with the blank one. **Rh1** (Rh content increased from 6.300 ± 0.929 to 625.166 ± 78.970 ng/10^6 cells) showed more dramatic increase than **Rh2** (Rh content increased from 6.300 ± 0.929 to 379.730 ± 45.860 ng/10^6 cells), indicating that **Rh1** containing fluorine atoms was more readily absorbed by cancer cells.[19]

The distribution of Rh in T-24 cells including cytoplasm, membrane, mitochondria, and nucleus fractions was detected after treatment with **Rh1** and **Rh2**. The highest Rh content was found in the cytoplasm, accounting for 73.82 and 44.17% of the total uptake of **Rh1** and **Rh2** by cells, respectively. The contents of Rh in the cell membrane, mitochondria, and nucleus were similar, which accounted for 10.40, 8.78, and 5.46% of the total **Rh1**, respectively, while the content of Rh in these three organelles accounted for 16.09, 11.04, and 5.03% of the total **Rh2**, respectively. These results showed that the two complexes entered tumor cells after 10 h of incubation, and their contents were different in each organelle fraction.

https://doi.org/10.1021/acs.jmedchem.3c00318
J. Med. Chem. 2023, 66, 9592−9606

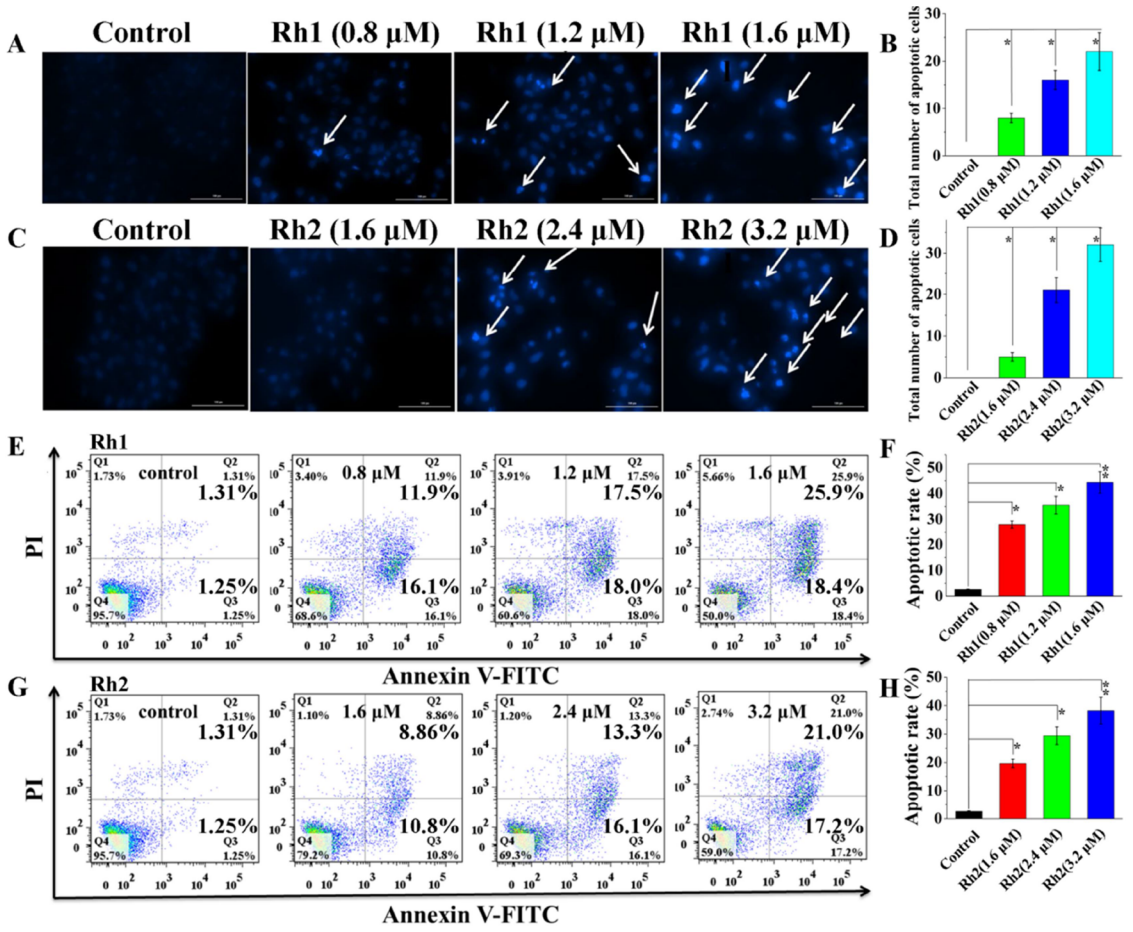

Figure 4. Hoechst 33258 staining of T-24 cancer cells incubated with **Rh1** (A, B) and **Rh2** (C, D) (24 h). Apoptosis of T-24 cancer cells induced by **Rh1** (E) and **Rh2** (G). Representative images and quantitative displays of apoptosis by **Rh1** (F) and **Rh2** (H).

DNA Damage and Cell Cycle Arrest. Since DNA is the main target by the metal complexes,[54] the effects of the complexes on DNA was first studied. Comet assay was used to detect DNA damage by **Rh1**, **Rh2**, and cisplatin (DDP) treatment in T-24 cancer cells (Figure 3). The cells in the control one were round in shape, but the cells showed comet-like tails after incubation for 24 h with different concentrations of the rhodium(III) complexes (Figure 3A,B). DNA damage was especially evident after treatment with **Rh1** (1.6 μM), which indicated that the complexes caused DNA fragmentation and might further induce cell apoptosis.

PARP-1 is widely recognized as a first-line molecule in DNA damage response.[55] H2AX (γ-H2AX) is essential for DNA repair after checkpoint-mediated cell cycle arrest and DNA double-strand break.[49] To further verify that **Rh1** and **Rh2** induced DNA damage, western blot analysis was employed to assess the expression changes of biomarkers connected with DNA damage. After the incubation of T-24 cancer cells with the rhodium(III) complexes for 48 h, the cleavage of PARP-1 (*c*-PARP) and γ-H2AX protein expressions was significantly increased (Figure 3C,D), suggesting that the rhodium(III) complexes killed cells by destroying DNA and that **Rh1** and **Rh2** were potential DNA-damaging agents. Moreover, cleavage of PARP (*c*-PARP) is known as a hallmark of apoptosis, which will be further investigated in subsequent studies.

Furthermore, to determine whether **Rh1** and **Rh2** interact with DNA, several methods were used to investigate their ability to bind to DNA. Relative to the rhodium(III) complex without calf thymus DNA (ct-DNA), the maximum absorption peak of **Rh1** was observed at 272 nm, and that of **Rh2** was 278 nm, which exhibited approximately 79.9 and 60.9% hypochromism (shown by the black arrow) with the increase of ct-DNA concentration, respectively. According to the fitting calculation of UV−vis spectral data, the binding constants of the two complexes were similar ($K_b = 1.12 \times 10^5$ M^{-1} and $K_b = 1.09 \times 10^5$ M^{-1}, respectively), indicating that **Rh1** and **Rh2** have a high DNA-binding affinity.[20,28] The maximum absorption peaks of the two complexes did not shift significantly (Figure S57A,B). Moreover, the fluorescence intensity of ethidium bromide-DNA (EB-DNA) significantly decreased with the increasing concentration of both the rhodium(III) complexes, suggesting that the rhodium(III) complex effectively competed with EB molecules for insertion sites on ct-DNA by substituting EB molecules (Figure S57C,D). These results indicated that **Rh1** and **Rh2** had strong interaction with DNA at a lower concentration, and they also caused damage to DNA when internalized in cells, as verified by the alkaline comet assay,[20,56] consistent with those of the abovementioned cellular experiments.

Effects of **Rh1** and **Rh2** on the cell cycle arrest of T-24 cells were investigated by flow cytometry analysis (Figure 3E,F). The results indicated that the G2/M phase distribution of tumor cells increased significantly in a concentration-dependent manner of **Rh1** and **Rh2**, which varied from 18.32 to 43.97 and 30.26%, respectively, while the proportion of S and G1 phase cells decreased simultaneously. These results reflected

https://doi.org/10.1021/acs.jmedchem.3c00318
J. Med. Chem. 2023, 66, 9592−9606

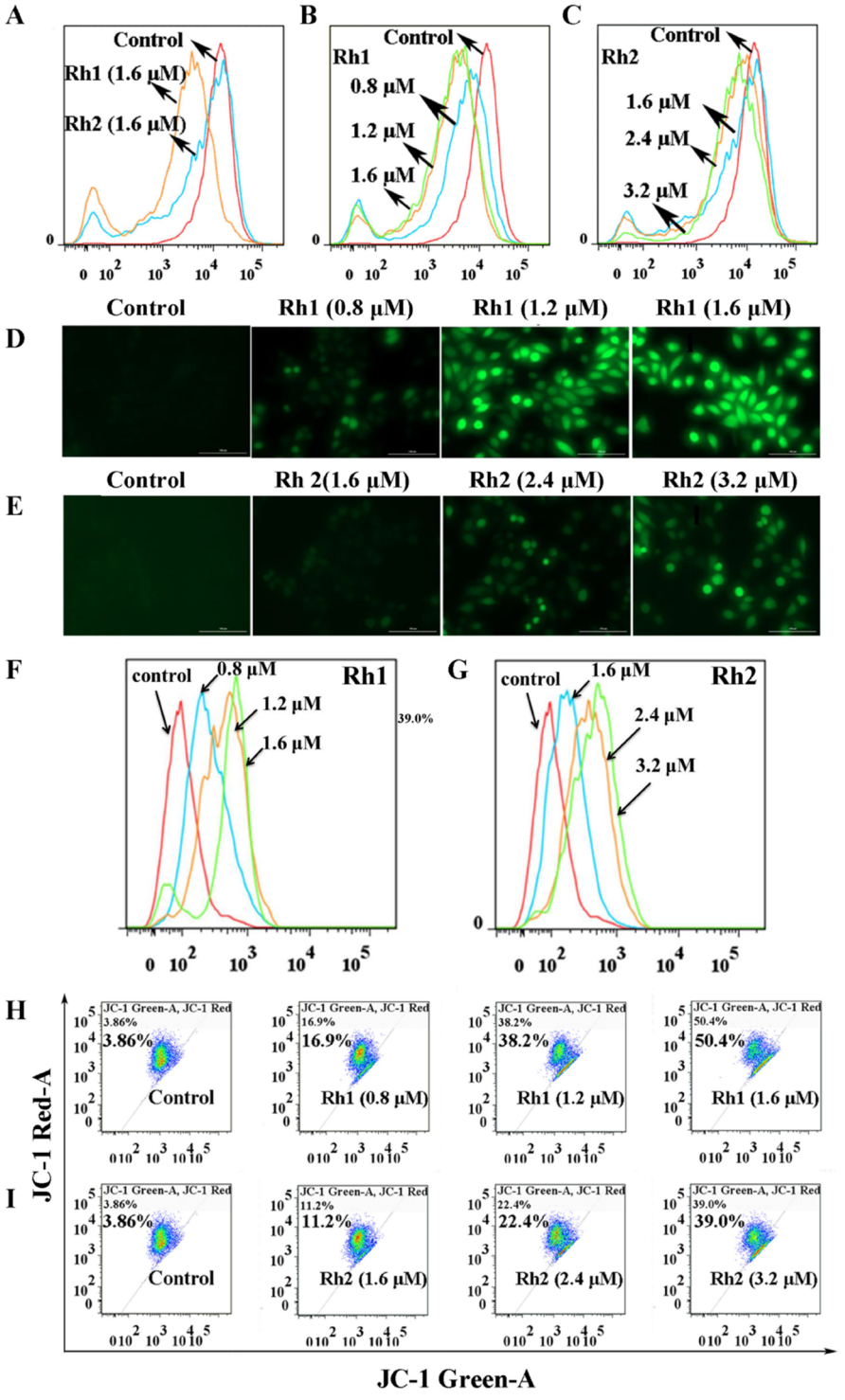

Figure 5. Detection of mPTP of T-24 cancer cells treated with **Rh1** and **Rh2** (A–C). ROS determination of cells after incubation with **Rh1** (D) and **Rh2** (E) was analyzed (12 h). Analysis of Ca^{2+} release in the cells upon treatment with **Rh1** (F) and **Rh2** (G) after 24 h. Influence of **Rh1** (H) and **Rh2** (I) on the MMP of T-24 cancer cells (24 h).

that the inhibition of **Rh1** and **Rh2** on T-24 cells might be through blocking the synthesis of cell DNA, causing G2/M phase cell cycle arrest, thereby inhibiting cell proliferation.[57]

The changes in G2-related proteins in T-24 cancer cells incubated with **Rh1** and **Rh2** for 48 h were studied by western blot (Figure 3G,H). Cyclin B, as a G2 phase-related protein, activates and forms complex with cyclin-dependent protein kinases (CDKs) to promote G2/M phase cell transformation,[15] and the expression level of cyclin B1 was gradually downregulated with increasing concentrations of the two complexes compared with the control one, resulting in G2/M phase arrest. CDK1, a cyclin-dependent kinase, was downregulated significantly and maintained in a nonactivated state, thereby blocking mitotic initiation, decreasing the expression level of CDC25C, and inhibiting the dephosphorylation of

https://doi.org/10.1021/acs.jmedchem.3c00318
J. Med. Chem. 2023, 66, 9592−9606

mitotic kinase CDK1/cyclin B1. These results showed that **Rh1** and **Rh2** arrested the T-24 cell cycle in the G2/M phase.

Apoptosis Induction. Apoptosis is a fundamental and inherent biological process that maintains the balance between cell proliferation and death.[58] Hoechst 33258 staining is commonly used to identify apoptotic cell DNA.[59] To observe the effects of **Rh1** and **Rh2** on cell apoptosis, the treated cells were stained and detected by fluorescence microscopy (Figure 4A−D), which showed that the apoptosis rates of T-24 cells were significantly increased after incubation with **Rh1** and **Rh2**. The cells in the treated group showed typical apoptotic cell morphological changes, including bright blue fluorescence, nuclear chromatin presenting a crescent shape, and shrunken nuclear membrane, in a concentration-dependent manner.

Quantitative measurement of **Rh1** and **Rh2** induced apoptosis by flow cytometry (Figure 4E−H). With the increase of the concentration of the rhodium(III) complexes, the percentage of cell apoptosis (Q2 + Q3) increased. When the concentration of **Rh1** was 0.8 and 1.6 μM, the proportion of apoptotic cells was 28.0 and 44.3%, respectively. A similar effect was observed for **Rh2**. When treated with **Rh2** (3.2 μM), the apoptosis rate of T-24 cancer cells changed from 2.56 to 38.2%.

Mitochondria-Mediated Apoptotic Pathway. Mitochondria are the bioenergetic and metabolic centers of cells, regulating intracellular homeostasis by controlling calcium signaling, energy production, and cellular metabolism, and mitochondrial damage may lead to apoptosis,[60] which is characterized by the opening of mitochondrial permeability transition pore (mPTP), elevated ROS, released Ca^{2+}, decreased MMP, and activation of caspase-3, caspase-8, and caspase-9.[61]

Effects on mPTP. The opening of mPTP is a vital event that causes cell death.[62] To elucidate the underlying mechanism of complex-induced apoptosis, we explored its possible effects on mitochondrial functions. The detection of mPTP indicated that **Rh1** and **Rh2** sharply increased the opening of mPTP (Figure 5A−C), which might trigger ROS imbalance and calcium homeostasis disruption, resulting in mitochondrial dysfunction.[62]

Effects on ROS. The release of ROS after the treatment of T-24 cancer cells with **Rh1** and **Rh2** for 12 h was detected by fluorescence microscopy after staining with the ROS (H_2O_2) probe DCFH-DA. The cells, complex-treated, showed enhanced green fluorescence with the increase of the concentration of complexes compared with the blank one (Figure 5D,E), suggesting that the release of ROS increased significantly. Furthermore, the cellular content of H_2O_2 was quantified by a hydrogen peroxide detection kit (Figure S58). The results showed that both **Rh1** and **Rh2** produced more H_2O_2 at the same concentration (1.6 μM) than did the control group, and the effect of **Rh1** was more obvious. These results indicated that **Rh1** and **Rh2** effectively caused the increase of ROS in T-24 cells, thus triggering cell apoptosis.[63,64]

Effects on the Intracellular Ca^{2+} Levels. Ca^{2+}, as a second messenger or death signal transduction molecule, mediates apoptosis through the activation of apoptosis-related protein kinases and nucleases.[65] Figure 5F,G shows that compared with the blank one (red peak), the intracellular Ca^{2+} level was increased after treatment with **Rh1** and **Rh2**. With the increase of the drug concentration, the intracellular Ca^{2+} level increased significantly, indicating that **Rh1** and **Rh2** effectively caused the increase of Ca^{2+} in T-24 cancer cells.

Effects on the Mitochondrial Membrane Potential. The effects of **Rh1** (0.8, 1.2, and 1.6 μM) and **Rh2** (1.6, 2.4, and 3.2 μM) on the mitochondrial membrane potential (MMP) of T-24 cells were also examined (Figure 5H,I). Compared with the control one, with the concentration of **Rh1** and **Rh2** increasing to 2 × IC_{50}, the mitochondrial membrane potential decreased from 3.86 to 50.4 and 39.0%, respectively. It could be concluded that both complexes significantly reduced the membrane potential of T-24 cells and activated the caspase cascade, finally leading to cell apoptosis.

Activation of Caspase-3, Caspase-8, and Caspase-9. After cytochrome *C* (Cytc) is released by mitochondria, caspase-9 forms a complex with Cytc and Apaf-1 and is simultaneously activated. Activated caspase-9 can activate caspase-3, the most vital enzyme for cell apoptosis, and then promote the subsequent apoptotic signaling pathway. Activation of caspase-3, caspase-8, and caspase-9 is important for the induction of apoptosis.[66] Figure S59 shows the activation of caspase-3, caspase-8, and caspase-9 by **Rh1** and **Rh2** in T-24 cells after incubation for 24 h. Compared with the blank one, the activity of caspase-3 and caspase-9 was obviously increased in the dose-supplemented group, while the change of caspase-8 was not obvious. The results indicated that **Rh1** and **Rh2** distinctly activated caspase-3 and caspase-9 of T-24 cancer cells to induce apoptosis. Therefore, we speculated that the main pathway of the two complexes inducing apoptosis of T-24 cancer cells was through the caspase-dependent pathway.[38]

In the mitochondria-mediated apoptosis pathway, Bcl-2 and caspase family proteins regulate cell apoptosis and promote the release of cytochrome *c* to activate the caspase cascade and induce cell death.[67] To further examine the molecular mechanism underlying the action of the compounds against T-24 cancer cells, the change of apoptosis-related proteins was measured by western blot (Figure 6A,B). The measured

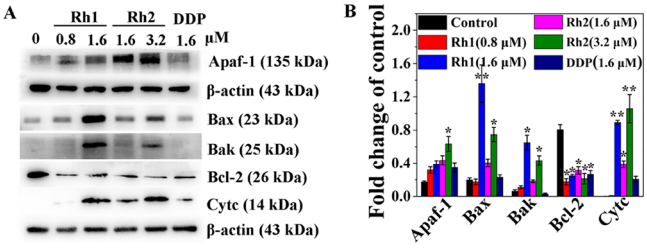

Figure 6. Change of apoptosis-related proteins after incubation with **Rh1** and **Rh2** in T-24 cells (48 h) detected by western blot (A). Histograms displaying the density ratios of the related proteins of apoptosis (B).

apoptotic proteins included Apaf-1, Bax, Bak, Bcl-2, and Cytc. As shown, compared with the control group, the expression level of anti-apoptotic protein Bcl-2 was decreased, while the expression level of proteins Apaf-1, Bax, Bak, and Cytc were increased, leading to MMP disruption and the release of Cytc into the cytoplasm to initiate the mitochondria-mediated pathway of apoptosis.[68] Cytoplasmic Cytc activates the initiator caspase-9 and the subsequent downstream effector caspase-3, which further cleaves PARP causing apoptosis. Cleavage of PARP-1 by caspases is considered a hallmark of apoptosis.[69] It is worth mentioning that the effects of **Rh1** and **Rh2** on related proteins were more obvious than those of cisplatin.

https://doi.org/10.1021/acs.jmedchem.3c00318
J. Med. Chem. 2023, 66, 9592−9606

Triggering Cell Autophagy. Autophagy degrades and recycles damaged or aged proteins and organelles and is a dynamic cellular pathway. It is closely associated with cancer promotion and prevention. Mitochondrial damage can induce autophagy or mitochondrial autophagy.[70] The autophagy detection kit was adopted to measure the autophagy of T-24 cells induced by **Rh1** and **Rh2**. Brighter blue spots were produced on autophagic vesicles in the complex-treated group (Figure 7A), which indicated that **Rh1** and **Rh2** caused autophagy in T-24 cancer cells.

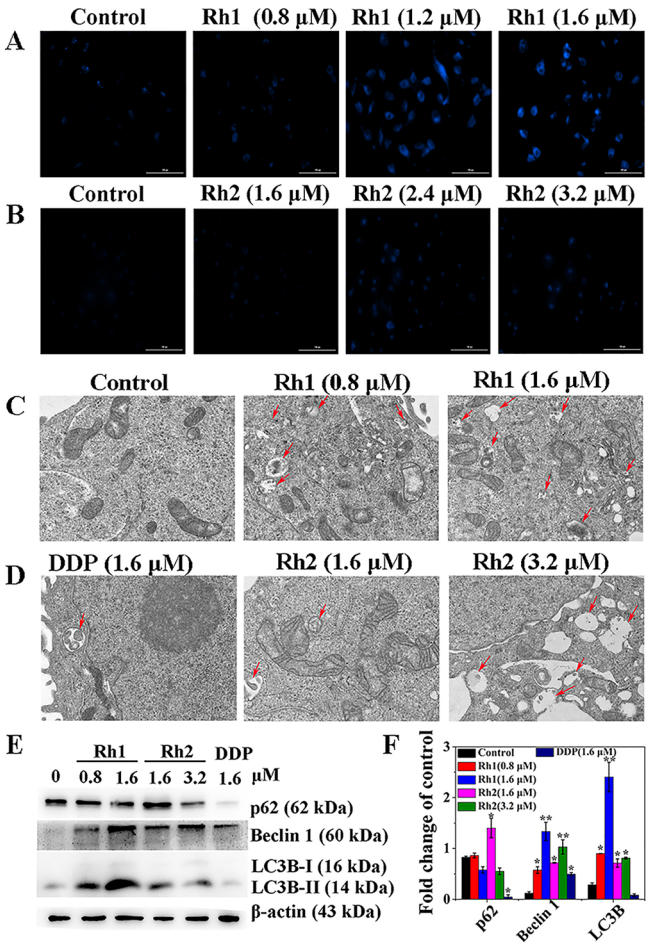

Figure 7. Autophagy determined in the T-24 cancer cells (A and B). Representative TEM images of T-24 cancer cells treated with **Rh1**, **Rh2**, and **DDP** for 48 h (C and D). Changes of the autophagy-related proteins after incubation with **Rh1** and **Rh2** were analyzed by western blot (48 h) (E). Histograms displaying the density ratios of autophagy-related proteins (F).

As an indicator of autophagy, vacuoles of autophagosomes can be observed in TEM images after treatment with **Rh1** (0.8 and 1.6 μM) and **Rh2** (1.6 and 3.2 μM) for 48 h (Figure 7B), and the number of vacuoles of autophagosomes rose with the increase in the complex concentration. Particularly, more vacuoles were formed after treatment with **Rh1** and **Rh2** than with cisplatin at the same concentration (1.6 μM).

The effect of autophagy on promoting tumor death is usually through autophagy-associated proteins, such as autophagy markers p62 and Beclin 1, and conversion of LC3-I to LC3-II.[71] During autophagy, LC3-I is modified and processed by a ubiquitin-like system to form LC3-II, which is an important marker of autophagosome.[72] Further evidence of autophagy was manifested by western blot (Figure 7C,D). It was found that the expression of autophagy markers LC3-II and Beclin 1 was upregulated. Meanwhile, the level of autophagy substrate p62/SQSTM1 was downregulated by the treatment with **Rh1** and **Rh2**, indicating that the protein was degraded in autophagosomes. These results confirmed that **Rh1** and **Rh2** significantly triggered autophagy in T-24 cancer cells.

Our study on the anticancer mechanism of **Rh1** and **Rh2** demonstrated that cycle arrest caused by DNA damage and mitochondrial damage induced by ROS accumulation are the main causes of apoptosis and autophagy.

In Vivo Anticancer Activity in Xenograft Tumor Model. The tumor suppression activity by **Rh1** and **Rh2** in vivo was investigated in nude mice (Balb/c) inoculated with T-24 cancer cells. The complexes were dosed via intravenous administration in the tail. The results showed that the tumor volume after incubation with **Rh1** at 7.5 and 15.0 mg/kg decreased, compared with the control one on the 15th day and 11th day, respectively (Figure 8). The tumor volume after

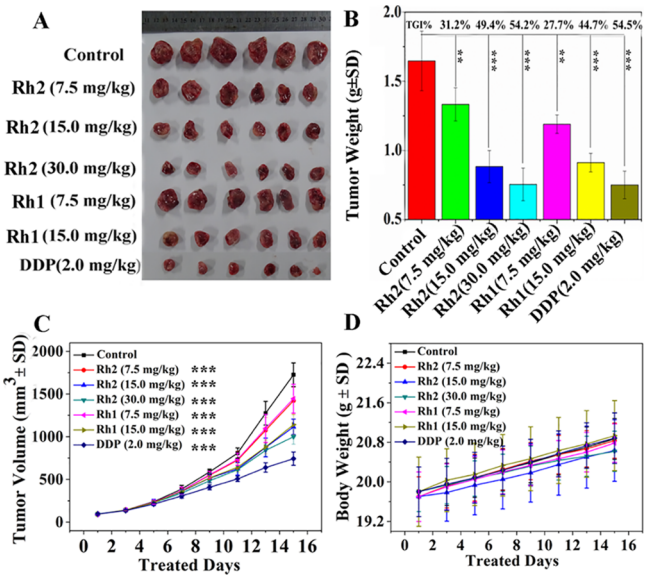

Figure 8. T-24 tumor growth suppressed by **Rh1** and **Rh2** in vivo. (A) Photographs of tumors isolated from the mice. (B) Weight of tumor was monitored. (C) Volume of tumors treated with **Rh1** and **Rh2**. (D) Body weight of the mice (mean tumor volume (mm^3) ± SD (n = 6).

treatment with **Rh2** at 7.5, 15.0, and 30.0 mg/kg decreased significantly on the 15th, 11th, and 9th day compared with the control one, with significant statistical differences. The volume of tumor in the cisplatin-treated area was significantly decreased on the 5th day after administration. After 15 days of drug treatment, the inhibitory rates of the different groups were 27.7, 44.7, 31.2, 49.4, and 54.2%, respectively (Figure 8A,B). These results suggested that the two complexes inhibited the growth of the human bladder cancer T-24 xenograft model and that **Rh2** has superior anticancer activity to **Rh1** (Figure 8C). At the same time, no obvious difference was observed in the body weight of nude mice treated with **Rh1** and **Rh2** (Figure 8D), compared with the control, indicating the in vivo safety of the complexes.

The spleen, liver, heart, kidney, lung, and tumor tissues of mice were collected and stained with H&E. It was observed

https://doi.org/10.1021/acs.jmedchem.3c00318
J. Med. Chem. 2023, 66, 9592−9606

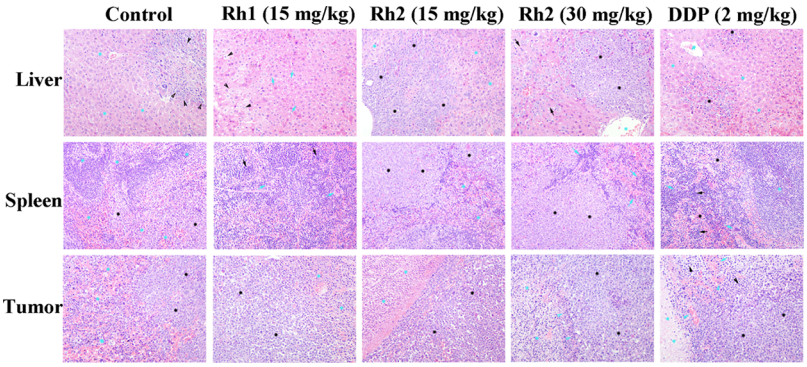

Figure 9. Histological examination of the liver, spleen, and tumor sections in tumor-bearing mice (magnification, 200×; black stars indicate tumor cells; black arrows indicate anomalous cells, which resemble tumor; blue stars in liver and spleen sections indicate normal tissue and those in tumor sections indicate tumor necrosis; blue arrows refer to multinucleated megakaryocytes, tumor cells, and necrotic tissue junction or vascular congestion and hemorrhage; and blue pentagrams refer to central veins).

that the structures of the lung, heart, and kidney of mice treated with **Rh1** and **Rh2** were normal, and no drug-related pathological damage was observed (Figure S60). Complex **Rh2** was slightly more toxic to the spleen, and the spleen structure was altered and filled with a large number of tumor cells. It was important to note that the control group and the three **Rh2**-treated groups showed different degrees of tumor spread to the liver and spleen; the DDP group showed mild liver metastasis; but, no tumor lesions were found in the spleen and liver tissues in the **Rh1**-treated (15.0 mg/kg) group (Figure 9). This observation suggested that **Rh1** (15 mg/kg) inhibited liver and spleen metastasis associated with T-24 tumors, and it had low toxicity for liver and spleen tissues. Overall, **Rh1** showed promise as a potent anticancer agent in vivo,[73] which is consistent with the inhibition of cell-invasive metastasis in vitro. Pathological examination of tumor sections showed that the number of inflammatory cells in each drug administration group was significantly higher than that in the control group. **Rh1** caused the most serious lesions. The different changes in cell morphology in each group are indicated by arrows or asterisks. Pathological examination records of five organs and tumors in T24 tumor-bearing nude are listed in Table S6.

Inhibition of Metastasis by Rhodium Complexes. The migration of cancer cells is a key step in cancer metastasis. Thus, suppressing the migration of cancer cells is an alternative strategy to treat cancer.[74] To determine whether **Rh1** and **Rh2** can inhibit the migration of cancer cells, wound healing (Figure 10A–D) and transwell tests (Figure 10E–H) were performed. The transwell test results showed that the two rhodium complexes significantly inhibited T-24 invasion at an IC_{50} concentration. In addition, adhesion experiments (Figure 10I–L) displayed that **Rh1** and **Rh2** suppressed the adhesion of T-24 cancer cells dose-dependently. Therefore, **Rh1** and **Rh2** strongly inhibited the migration, invasion, and adhesion of T-24 cancer cells in vitro.[57]

MMP-2 and MMP-9 are key biomarkers for the prognosis of cancer metastasis.[74] FAK plays a crucial role in the early stages of cell migration and adhesion; integrin β1 and EGFR are closely associated with radio resistance, mobility of cancer cells, and tumor cell growth, migration, and adhesion.[57,73] To elucidate the possible mechanisms of metastasis inhibition by **Rh1** and **Rh2**, some related proteins were detected by western blot. As shown in Figure 10M,N, the two complexes reduced the levels of MMP-9 and MMP-2, indicating that **Rh1** and **Rh2** have antimetastasis potential, which is consistent with the wound healing experiment results. Meanwhile, the level of FAK protein expression did not change, but FAK phosphorylation (at the Tyr397 residue) was inhibited effectively. Integrin β1 and EGFR levels were obviously decreased after incubation with **Rh1** and **Rh2**. These results indicated that **Rh1** and **Rh2** inhibited the metastasis of T-24 cancer cells and could be used as antimetastasis agents.

Inhibition of Lung Metastasis In Vivo. Furthermore, the antimetastasis activity of **Rh1** and **Rh2** in vivo was confirmed, and mouse lung cancer cells 4T1 were injected into the tail vein to establish an experimental lung metastasis model. Significant metastases were observed in the control group, with more metastatic nodules on the lung surface. However, the mice treated with **Rh1** and **Rh2** showed a reduced number of metastatic nodules in the lungs due to the combined inhibition of tumor growth and metastasis. Importantly, the **Rh1** treatment is more effective (Figure 11A). H&E staining of the lungs further indicated that treatment with **Rh1** and **Rh2** significantly reduced the area of micrometastatic lesions (Figure 11B,C). These results confirmed the antimetastatic activity of **Rh1** and **Rh2** in vivo.

CONCLUSIONS

Eleven rhodium(III)-picolinamide complexes were synthesized and characterized, which showed high cytotoxicity to five cancer cell lines and less toxicity to WI38 normal cells. Mechanism studies revealed that **Rh1** and **Rh2** suppressed cell proliferation and inhibited cancer cell metastasis via multiple modes of action such as cell cycle arrest, apoptosis, and autophagy. They induced DNA damage and arrested the cell cycle in the G2/M phase and altered the expression levels of cycle-related proteins, caused apoptosis by opening the mitochondrial permeability transition pore, elevating the levels of intracellular ROS and free calcium, reducing MMP, and activating the caspase cascade. The two complexes exhibited efficient in vivo anticancer activity in a T-24 tumor xenograft model. In addition, they showed high anticancer and antimetastasis effects in vivo. They reduced MMP-2/9-, EGFR-, and EMT-related proteins by inhibiting the integrin-focal adhesion kinase signaling pathway, thereby inhibiting the tumor cell migration, invasion, and adhesion. Overall, the picolinamide-based Rh(III) complexes **Rh1** and **Rh2** are promising therapeutic agents due to their high antiproliferative and antimetastatic activities against cancer cells, with low toxicity on normal cells.

https://doi.org/10.1021/acs.jmedchem.3c00318
J. Med. Chem. 2023, 66, 9592−9606

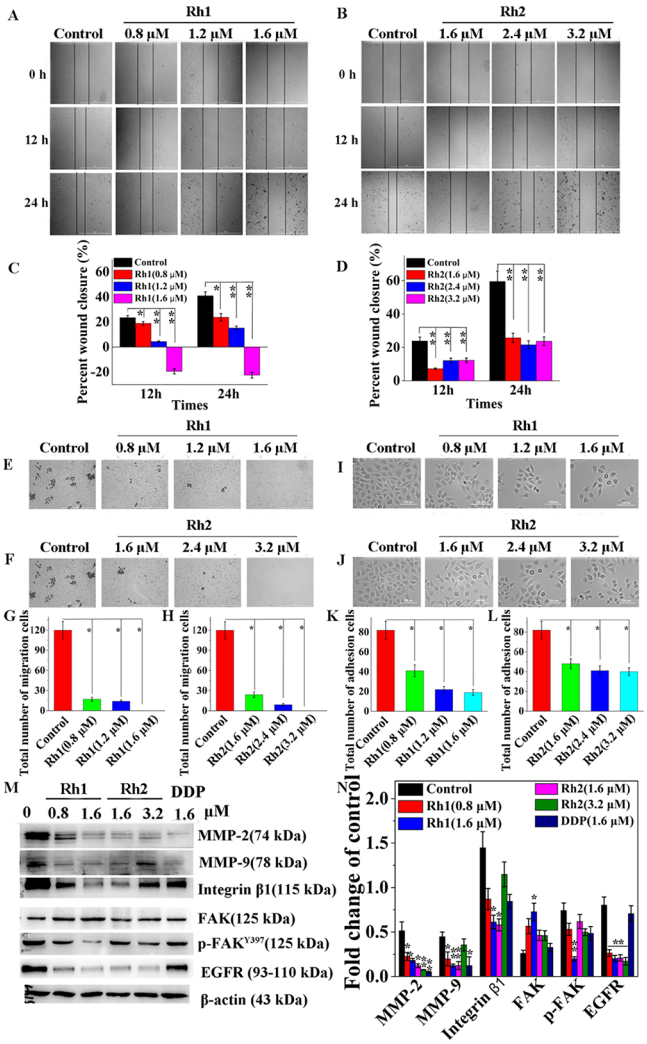

Figure 10. Scratches of T-24 cancer cells were induced with pipette tips (10 μL). After 12 or 24 h of incubation with **Rh1** (A, C) and **Rh2** (B, D), images were photographed under a phase contrast microscope. T-24 cancer cells were seeded onto chambers and incubated with **Rh1** (E, G) and **Rh2** (F, H) (24 h). T-24 cells were treated with **Rh1** (I and K) and **Rh2** (J and L) in six-well plates (24 h), nonadherent cells were washed off with PBS, and the adhesive cells were captured under a phase contrast microscope. (M) Changes of migration-related biomarkers treated with **Rh1** and **Rh2** were analyzed by western blot (48 h). (N) Histograms displaying the density ratios of migration-related proteins.

EXPERIMENTAL SECTION

Unless otherwise indicated, all chemicals were obtained from commercial companies. Other biochemical materials are listed in the Supporting Information. All synthesized compounds were dried before testing. The purity of all rhodium(III) complexes used in the experiments was >95%, which was routinely verified by HPLC. The animal experiments were approved by the ethics committee for laboratory animals, the Nanjing Han & Zaenker Cancer Institute, Nanjing OG Pharmaceuticals, Co., Ltd. (SYXK(SU)2017-0040). The animal experiments were performed in accordance with the NIH Guidelines for the Care and Use of Laboratory Animals.

Synthesis of Ligands. The picolinamide ligands were prepared according to the literature method.[46,75] All other reagents are commercially available and were used as received. The characterization data of ligands are presented in the Supporting Information.

Synthesis of Rhodium Complexes Rh1−Rh11. The reactions of picolinamide ligands with $RhCl_3{\cdot}3H_2O$ (Adamas) were carried out

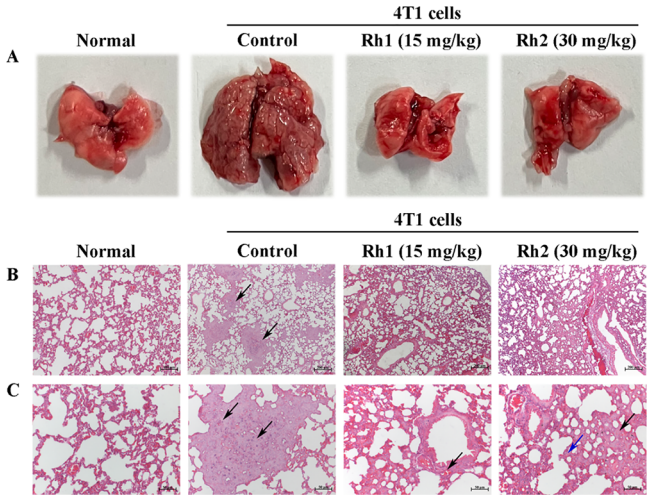

Figure 11. In vivo **Rh1** and **Rh2** inhibited lung metastasis. (A) Pictures of representative lesions for 4T1 tumor metastasis on the lung surface from complex-treated mice on day 14. (B and C) H&E staining images of the lung surface tumor metastases in 14 days' old mice treated with **Rh1** and **Rh2** (magnification 50× and 200×, respectively).

in the presence of CH_3CN/CH_3OH (v:v = 4:1, 10 mL) under solvothermal conditions. The reactions were maintained in a 100 °C oven for 3 days, cooled slowly to room temperature, and filtered, and the filtrate was placed in a 50 mL beaker and slowly volatilized for 3−5 days until the crystal was precipitated. Reddish brown crystals of **Rh1−Rh11** were formed, and the structures were detected by the single-crystal X-ray diffraction method, HRMS spectroscopy, NMR spectroscopy, elemental analysis, and powder X-ray diffraction analysis; the characterization data of **Rh1−Rh11** are presented in the Supporting Information. The purity of all complexes was higher than 95%, as observed by HPLC (Figure S51).

MMP Measurement. T-24 cancer cells were cultivated and incubated with the complexes; after 24 h, the cells were harvested. The collected cells were stained with JC-1 (1.0 μg/mL) for 20 min in PBS in the dark, collected by centrifugation, and cleaned with PBS. Flow cytometry was used to detect the ratio of red to green fluorescence intensity of the resuspension cells in PBS.

Autophagy Induced by Complexes. T-24 cancer cells (2×10^5 cells/well) were cultivated in plates overnight; then, **Rh1** and **Rh2** were added, respectively, at the specified concentration for 24 h. The cells were collected and cleaned; the detection reagent of the cell and autophagosome (1×, 500 μL) were added; incubated in an incubator for 15 min; and washed. Then, the cells were observed and photographed with a fluorescence microscope.

TEM Images. T-24 cells (5×10^6 cells) were cultivated in a dish (100 mm) overnight and treated with **Rh1** and **Rh2** (24 h). After removing the medium, 2.5% glutaraldehyde was added to fix the cells at 25 °C for about 5 min. The cells were gently scraped down in one direction with a cell scraper, centrifuged, collected, and fixed with 2.5% glutaraldehyde overnight. 1% osmium was added to fix the cells at 4 °C for 1 h, followed by gradient dehydration, and the resin was embedded for 24 h. The samples were cut into 60−80 nm thickness using a Leica EM UC6 ultramicrotome and collected on an elliptical copper grid (Hatfield, PA, USA), followed by staining with 2% aqueous uranyl acetate and lead citrate. Subsequently, the samples were cleaned and placed under a Hitachi7500 fluoroscopic electron microscope (Philips, Amsterdam, The Netherlands) to observe the ultrastructural morphology and status of autophagolysosomes and lysosomes in each group of cells after drying.

Acute Toxicity Study. Balb/c nude mice (half male and half female) were divided randomly into two groups, with six animals in each group, namely, the **Rh1** (0.5 mg/mL) group and the **Rh2** (1.25 mg/mL) group. After 1 week of adaptive feeding, each group was

https://doi.org/10.1021/acs.jmedchem.3c00318
J. Med. Chem. 2023, 66, 9592−9606

injected with the correspondingly prepared drug solution (94% normal saline, 5% DMSO, and 1% Tween-80) by a single intravenous administration through tail. The animals were observed, and the number of deaths was recorded, while the survived animals were observed for a week.

Animal Experiments. A total of 55 Balb/c nude mice (5×10^6 cells per mouse) were inoculated subcutaneously under the right axillary with a suspension of T-24 cancer cells at the logarithmic growth stage. When the tumor grew to about 100 mm^3, 42 tumor-bearing nude mice with a healthy growth status and almost the same tumor size were divided into seven groups randomly (six mice per group). Control group, **Rh1** (7.5 mg/kg) group, **Rh1** (15.0 mg/kg) group, **Rh2** (7.5 mg/kg) group, **Rh2** (15.0 mg/kg) group, **Rh2** (30.0 mg/kg) group, and DDP (2.0 mg/kg) group were dosed via tail intravenous administration according to the dose-setting table (0.2 mL per mouse, once every other day). Nude mice's body weight and tumor diameter were measured and recorded every other day. After administration for 2 weeks, the nude mice were killed by neck dissection. The tissues of tumor and viscera were removed and fixed with 10% neutral formalin. The tumor tissues were weighed, and the tumor inhibition rate was calculated. One sample of organ and tumor was randomly selected for tissue sections. Histopathological studies were conducted after H&E staining.

Inhibition of Lung Metastasis. 4T1 cells were resuscitated in serum-free medium and were injected with 5×10^5 cells/0.2 mL culture medium through the tail vein, and the mice were immediately treated with **Rh1** and **Rh2** at 15 or 30 mg/kg dosage. Two weeks later, the animals were killed, and lungs were fixed in liquid nitrogen; then, the number of metastatic nodules on the lung surface was calculated.

Statistical Studies. To ensure reliability of data, every experiment was repeated three times (the control group was treated with blank solution), and the data of the results were expressed as mean ± standard deviation (SD), $^{***}P < 0.001$, $^{**}P < 0.01$, and $^{*}P < 0.05$.

■ ASSOCIATED CONTENT

Supporting Information

The Supporting Information is available free of charge at https://pubs.acs.org/doi/10.1021/acs.jmedchem.3c00318.

HRMS, ^{1}H NMR, and ^{13}C NMR spectra of ligands **3a**−**3k**; HRMS spectra, X-ray crystallography, HPLC, and UV−vis spectra of **Rh1**−**Rh11**; cytotoxicity in vitro; cell viability analysis; lipophilicity measurement; cell apoptosis; cell cycle studies; comet assay; ROS; Ca^{2+} of intracellular determination; Hoechst staining; caspase 3, caspase 8, and caspase 9 assay; migration detection; western blot; and H&E staining (PDF)

Molecular formula strings (CSV)

■ AUTHOR INFORMATION

Corresponding Authors

Hong Liang − *State Key Laboratory for Chemistry and Molecular Engineering of Medicinal Resources, Collaborative Innovation Centre for Guangxi Ethnic Medicine, School of Chemistry and Pharmaceutical Sciences, Guangxi Normal University, Guilin 541004, P. R. China*; Email: hliang@gxnu.edu.cn

Zhen-Feng Chen − *State Key Laboratory for Chemistry and Molecular Engineering of Medicinal Resources, Collaborative Innovation Centre for Guangxi Ethnic Medicine, School of Chemistry and Pharmaceutical Sciences, Guangxi Normal University, Guilin 541004, P. R. China*; orcid.org/0000-0002-6548-6131; Email: chenzf@gxnu.edu.cn

Authors

Yun-Qiong Gu − *State Key Laboratory for Chemistry and Molecular Engineering of Medicinal Resources, Collaborative Innovation Centre for Guangxi Ethnic Medicine, School of Chemistry and Pharmaceutical Sciences, Guangxi Normal University, Guilin 541004, P. R. China; School of Environment and Life Science, Nanning Normal University, Nanning 530001, P. R China*

Kun Yang − *State Key Laboratory for Chemistry and Molecular Engineering of Medicinal Resources, Collaborative Innovation Centre for Guangxi Ethnic Medicine, School of Chemistry and Pharmaceutical Sciences, Guangxi Normal University, Guilin 541004, P. R. China*

Qi-Yuan Yang − *State Key Laboratory for Chemistry and Molecular Engineering of Medicinal Resources, Collaborative Innovation Centre for Guangxi Ethnic Medicine, School of Chemistry and Pharmaceutical Sciences, Guangxi Normal University, Guilin 541004, P. R. China*

Huan-Qing Li − *State Key Laboratory for Chemistry and Molecular Engineering of Medicinal Resources, Collaborative Innovation Centre for Guangxi Ethnic Medicine, School of Chemistry and Pharmaceutical Sciences, Guangxi Normal University, Guilin 541004, P. R. China*

Mei-Qi Hu − *State Key Laboratory for Chemistry and Molecular Engineering of Medicinal Resources, Collaborative Innovation Centre for Guangxi Ethnic Medicine, School of Chemistry and Pharmaceutical Sciences, Guangxi Normal University, Guilin 541004, P. R. China*

Meng-Xue Ma − *State Key Laboratory for Chemistry and Molecular Engineering of Medicinal Resources, Collaborative Innovation Centre for Guangxi Ethnic Medicine, School of Chemistry and Pharmaceutical Sciences, Guangxi Normal University, Guilin 541004, P. R. China*

Nan-Feng Chen − *State Key Laboratory for Chemistry and Molecular Engineering of Medicinal Resources, Collaborative Innovation Centre for Guangxi Ethnic Medicine, School of Chemistry and Pharmaceutical Sciences, Guangxi Normal University, Guilin 541004, P. R. China*

Yang-Han Liu − *State Key Laboratory for Chemistry and Molecular Engineering of Medicinal Resources, Collaborative Innovation Centre for Guangxi Ethnic Medicine, School of Chemistry and Pharmaceutical Sciences, Guangxi Normal University, Guilin 541004, P. R. China*

Complete contact information is available at: https://pubs.acs.org/10.1021/acs.jmedchem.3c00318

Author Contributions

The manuscript was written through contributions of all authors. All authors have given approval to the final version of the manuscript.

Notes

The authors declare no competing financial interest.

■ ACKNOWLEDGMENTS

This work was supported by the National Natural Science Foundation of China (grant no. 22077022) and Natural Science Foundation of Guangxi Province of China (grant nos. GUIKEZY22096015, 2023GXNSFDA026054, and AD17129007).

ABBREVIATIONS

Apaf-1, apoptotic protease activating factor-1; **Bax**, Bcl-2-associated X; **Bak**, Bcl2, antagonist/killer; **Bcl-2**, B-cell lymphoma-2; **CDC25C**, cell division cycle 25C; **CDKs**, cyclin-dependent protein kinases; *c*-**PARP**, cleavage of PARP; C-raf, *c-Rafinhibitor*; **DCFH**, 2′,7′-dichlorofluorescein; **DMF**, N,N-dimethylformamide; **DMSO**, dimethyl sulfoxide; **DNA**, deoxyribonucleic acid; **EB**, ethidium bromide; **EGFR**, epidermal growth factor receptor; **FITC**, fluorescein isothiocyanate; **HPLC**, high-performance liquid chromatography; **γ-H2AX**, histone H2AX phosphorylation; **ICP-MS**, inductively coupled plasma mass spectrometry; $\mathbf{IC_{50}}$, half-maximal inhibitory concentrations; **JC-1**, 5,5′,6,6′-tetra-chloro-1,1′,3,3′-tetraethylbenzimidazolylcarbocyanine; **mPTP**, mitochondrial permeability transition pore; **MTT**, 3-(4,5-dimethylthiazol-2-yl)-2,5-diphenyltetrazolium bromide; **PBS**, phosphate-buffered saline; **PI**, propidium iodide; **ROS**, reactive oxygen species; $\mathbf{SOCl_2}$, thionyl chloride; **SAR**, structure−activity relationship; SD, standard deviation; **TEM**, transmission electron microscopy; **T/C**, relative tumor growth rate; **UV−Vis**, UV−visible.

REFERENCES

(1) Malandrino, A.; Kamm, R. D. In vitro modeling of mechanics in cancer metastasis. *ACS Biomater Sci. Eng.* **2018**, *4* (2), 294−301.

(2) Kittiwattanokhun, A.; Samosorn, S.; Innajak, S.; Watanapokasin, R. Inhibitory effects on chondrosarcoma cell metastasis by Senna alata extract. *Biomed. Pharmacother.* **2021**, *137*, 111337−111345.

(3) Diaz Arguello, O. A.; Haisma, H. J. Apoptosis-inducing TNF s superfamily ligands for cancer therapy. *Cancers* **2021**, *13* (7), 1543−1564.

(4) Merkul, E.; Muns, J. A.; Sijbrandi, N. J.; Houthoff, H. J.; Nijmeijer, B.; van Rheenen, G.; Reedijk, J.; van Dongen, G. An efficient conjugation approach for coupling drugs to native antibodies *via* the Pt(II) linker Lx for improved manufacturability of antibody-drug conjugates. *Angew. Chem., Int. Ed.* **2021**, *60* (6), 3008−3015.

(5) Castaneda, M.; den Hollander, P.; Kuburich, N. A.; Rosen, J. M.; Mani, S. A. Mechanisms of cancer metastasis. *Semin. Cancer Biol.* **2022**, *87*, 17−31.

(6) Liu, Y.; Li, S.; Liu, H.; Li, B. Osteogenic peptides in collagen hydrolysates: Stimulate differentiation of MC3T3-E1 cells *via* β1 integrin-FAK-ERK1/2 signaling pathway and Smad1 protein. *Food Biosci.* **2022**, *47*, 101775−101784.

(7) Brockmueller, A.; Mueller, A. L.; Shayan, P.; Shakibaei, M. Beta1-integrin plays a major role in resveratrol-mediated anti-invasion effects in the CRC microenvironment. *Front. Pharmacol.* **2022**, *13*, 978625−978742.

(8) Huang, T.; Meng, F.; Huang, H.; Wang, L.; Wang, L.; Liu, Y.; Liu, Y.; Wang, J.; Li, W.; Zhang, J.; Liu, Y. GALNT8 suppresses breast cancer cell metastasis potential by regulating EGFR O-GalNAcylation. *Biochem. Biophys. Res. Commun.* **2022**, *601*, 16−23.

(9) Li, X.; Zhao, L.; Chen, C.; Nie, J.; Jiao, B. Can EGFR be a therapeutic target in breast cancer? *Biochim. Biophys. Acta, Rev. Cancer* **2022**, *1877* (5), 188789−188801.

(10) Lv, P. C.; Jiang, A. Q.; Zhang, W. M.; Zhu, H. L. FAK inhibitors in cancer, a patent review. *Expert. Opin. Ther. Pat.* **2018**, *28* (2), 139−145.

(11) Li, Y.; Yang, G.; Zhang, J.; Tang, P.; Yang, C.; Wang, G.; Chen, J.; Liu, J.; Zhang, L.; Ouyang, L. Discovery, synthesis, and evaluation of highly selective vascular endothelial growth factor receptor 3 (VEGFR3) inhibitor for the potential treatment of metastatic triple-negative breast cancer. *J. Med. Chem.* **2021**, *64* (16), 12022−12048.

(12) Tang, J.; Zhang, J.; Liu, Y.; Liao, Q.; Huang, J.; Geng, Z.; Xu, W.; Sheng, Z.; Lee, G.; Zhang, Y.; Chen, J.; Zhang, L.; Qiu, X. Lung squamous cell carcinoma cells express non-canonically glycosylated IgG that activates integrin-FAK signaling. *Cancer Lett.* **2018**, *430*, 148−159.

(13) Shen, M.; Jiang, Y. Z.; Wei, Y.; Ell, B.; Sheng, X.; Esposito, M.; Kang, J.; Hang, X.; Zheng, H.; Rowicki, M.; Zhang, L.; Shih, W. J.; Celià-Terrassa, T.; Liu, Y.; Cristea, I.; Shao, Z. M.; Kang, Y. Tinagl1 suppresses triple-negative breast cancer progression and metastasis by simultaneously inhibiting integrin/FAK and EGFR signaling. *Cancer Cell* **2019**, *35* (1), 64−80.e67, DOI: 10.1016/j.ccell.2018.11.016.

(14) Scarim, C. B.; Lira de Farias, R.; de Godoy, Vieira; Netto, A.; Chin, C. M.; Leandro Dos Santos, J.; Pavan, F. R. Recent advances in drug discovery against mycobacterium tuberculosis: Metal-based complexes. *Eur. J. Med. Chem.* **2021**, *214*, 113166−113197.

(15) Xu, Z.; Kong, D.; He, X.; Guo, L.; Ge, X.; Liu, X.; Zhang, H.; Li, J.; Yang, Y.; Liu, Z. Mitochondria-targeted half-sandwich ruthenium^{II} diimine complexes: anticancer and antimetastasis *via* ROS-mediated signalling. *Inorg. Chem. Front.* **2018**, *5* (9), 2100−2105.

(16) Rubio, A. R.; Gonzalez, R.; Busto, N.; Vaquero, M.; Iglesias, A. L.; Jalon, F. A.; Espino, G.; Rodriguez, A. M.; Garcia, B.; Manzano, B. R. Anticancer activity of half-sandwich Ru, Rh and Ir complexes with chrysin derived ligands: Strong effect of the side chain in the ligand and influence of the metal. *Pharmaceutics* **2021**, *13* (10), 1540−1565.

(17) Zhou, X. Q.; Xiao, M.; Ramu, V.; Hilgendorf, J.; Li, X.; Papadopoulou, P.; Siegler, M. A.; Kros, A.; Sun, W.; Bonnet, S. The self-assembly of a cyclometalated palladium photosensitizer into protein-stabilized nanorods triggers drug uptake in vitro and in vivo. *J. Am. Chem. Soc.* **2020**, *142* (23), 10383−10399.

(18) Komor, A. C.; Barton, J. K. An unusual ligand coordination gives rise to a new family of rhodium metalloinsertors with improved selectivity and potency. *J. Am. Chem. Soc.* **2014**, *136* (40), 14160−14172.

(19) Komor, A. C.; Schneider, C. J.; Weidmann, A. G.; Barton, J. K. Cell-selective biological activity of rhodium metalloinsertors correlates with subcellular localization. *J. Am. Chem. Soc.* **2012**, *134* (46), 19223−19233.

(20) Aguirre, J. D.; Angeles-Boza, A. M.; Chouai, A.; Pellois, J. P.; Turro, C.; Dunbar, K. R. Live cell cytotoxicity studies: documentation of the interactions of antitumor active dirhodium compounds with nuclear DNA. *J. Am. Chem. Soc.* **2009**, *131* (32), 11353−11360.

(21) Sohrabi, M.; Bikhof Torbati, M.; Lutz, M.; Meghdadi, S.; Farrokhpour, H.; Amiri, A.; Amirnasr, M. Application of cyclometalated rhodium(III) complexes as therapeutic agents in biomedical and luminescent cellular imaging. *J. Photochem. Photobiol., A* **2022**, *423*, 113573−113585.

(22) Ohata, J.; Ball, Z. T. Rhodium at the chemistry-biology interface. *Dalton. Trans.* **2018**, *47* (42), 14855−14860.

(23) Zhong, H. J.; Wang, W.; Kang, T. S.; Yan, H.; Yang, Y.; Xu, L.; Wang, Y.; Ma, D. L.; Leung, C. H. A rhodium(III) complex as an inhibitor of neural precursor cell expressed, developmentally down-regulated 8-activating enzyme with in vivo activity against inflammatory bowel disease. *J. Med. Chem.* **2017**, *60* (1), 497−503.

(24) Sohrabi, M.; Saeedi, M.; Larijani, B.; Mahdavi, M. Recent advances in biological activities of rhodium complexes: Their applications in drug discovery research. *Eur. J. Med. Chem.* **2021**, *216*, 113308−113332.

(25) Legina, M. S.; Nogueira, J. J.; Kandioller, W.; Jakupec, M. A.; Gonzalez, L.; Keppler, B. K. Biological evaluation of novel thiomaltol-based organometallic complexes as topoisomerase IIalpha inhibitors. *J. Biol. Inorg. Chem.* **2020**, *25* (3), 451−465.

(26) Yang, G. J.; Wang, W.; Mok, S. W. F.; Wu, C.; Law, B. Y. K.; Miao, X. M.; Wu, K. J.; Zhong, H. J.; Wong, C. Y.; Wong, V. K. W.; Ma, K. L.; Leung, C. H. Selective inhibition of lysine-specific demethylase 5A (KDM5A) using a rhodium(III) complex for triple-negative breast cancer therapy. *Angew. Chem., Int. Ed.* **2018**, *57* (40), 13091−13095.

(27) Yang, C.; Wang, W.; Liang, J. X.; Li, G.; Vellaisamy, K.; Wong, C. Y.; Ma, D. L.; Leung, C. H. A rhodium(III)-based inhibitor of lysine-specific histone demethylase 1 as an epigenetic modulator in prostate cancer cells. *J. Med. Chem.* **2017**, *60* (6), 2597−2603.

https://doi.org/10.1021/acs.jmedchem.3c00318
J. Med. Chem. 2023, 66, 9592−9606

(28) Nano, A.; Boynton, A. N.; Barton, J. K. A Rhodium-cyanine fluorescent probe: Detection and signaling of mismatches in DNA. *J. Am. Chem. Soc.* **2017**, *139* (48), 17301−17304.
(29) Ernst, R. J.; Song, H.; Barton, J. K. DNA mismatch binding and antiproliferative activity of rhodium metalloinsertors. *J. Am. Chem. Soc.* **2009**, *131* (6), 2359−2366.
(30) Peerzada, M. N.; Hamel, E.; Bai, R.; Supuran, C. T.; Azam, A. Deciphering the key heterocyclic scaffolds in targeting microtubules, kinases and carbonic anhydrases for cancer drug development. *Pharmacol. Ther.* **2021**, *225*, 107860−107884.
(31) Sharma, V.; Gupta, M.; Kumar, P.; Sharma, A. A comprehensive review on fused heterocyclic as DNA intercalators: Promising anticancer agents. *Curr. Pharm. Des.* **2021**, *27* (1), 15−42.
(32) Moku, B.; Ravindar, L.; Rakesh, K. P.; Qin, H. L. The significance of N-methylpicolinamides in the development of anticancer therapeutics: Synthesis and structure-activity relationship (SAR) studies. *Bioorg. Chem.* **2019**, *86*, 513−537.
(33) Husseiny, E. M. Synthesis, cytotoxicity of some pyrazoles and pyrazolo[1,5-a]pyrimidines bearing benzothiazole moiety and investigation of their mechanism of action. *Bioorg. Chem.* **2020**, *102*, 104053−104068.
(34) Zeidan, M. A.; Mostafa, A. S.; Gomaa, R. M.; Abou-Zeid, L. A.; El-Mesery, M.; El-Sayed, M. A.; Selim, K. B. Design, synthesis and docking study of novel picolinamide derivatives as anticancer agents and VEGFR-2 inhibitors. *Eur. J. Med. Chem.* **2019**, *168*, 315−329.
(35) Garris, C.; Pittet, M. J. Therapeutically reeducating macrophages to treat GBM. *Nat. Med.* **2013**, *19* (10), 1207−1208.
(36) Dai, Y.; Hartandi, K.; Ji, Z.; Ahmed, A. A.; Albert, D. H.; Bauch, J. L.; Bouska, J. J.; Bousquet, P. F.; Cunha, G. A.; Glaser, K. B.; Harris, C. M.; Hickman, D.; Guo, J.; Li, J.; Marcotte, P. A.; Marsh, K. C.; Moskey, M. D.; Martin, R. L.; Olson, A. M.; Osterling, D. J.; Pease, L. J.; Soni, N. B.; Stewart, K. D.; Stoll, V. S.; Tapang, P.; Reuter, D. R.; Davidsen, S. K.; Michaelides, M. R. Discovery of N-(4-(3-amino-1H-indazol-4-yl)phenyl)-N'-(2-fluoro-5-methylphenyl)urea (ABT-869), a 3-aminoindazole-based orally active multitargeted receptor tyrosine kinase inhibitor. *J. Med. Chem.* **2007**, *50* (7), 1584−1597.
(37) Wang, L.; Zheng, Y.; Li, D.; Yang, J.; Lei, L.; Yan, W.; Zheng, W.; Tang, M.; Shi, M.; Zhang, R.; Cai, X.; Ni, H.; Ma, N. X.; Li, N.; Hong, F.; Ye, H.; Chen, L. Design, Synthesis, and Bioactivity Evaluation of Dual-Target Inhibitors of Tubulin and Src Kinase Guided by Crystal Structure. *J. Med. Chem.* **2021**, *64* (12), 8127−8141.
(38) Liu, M.; Liang, Y.; Zhu, Z.; Wang, J.; Cheng, X.; Cheng, J.; Xu, B.; Li, R.; Liu, X.; Wang, Y. Discovery of novel aryl carboxamide derivatives as hypoxia-inducible factor 1alpha signaling inhibitors with potent activities of anticancer metastasis. *J. Med. Chem.* **2019**, *62* (20), 9299−9314.
(39) Thangarasu, P.; Manikandan, A.; Thamaraiselvi, S. Discovery, synthesis and molecular corroborations of medicinally important novel pyrazoles; drug efficacy determinations through in silico, in vitro and cytotoxicity validations. *Bioorg. Chem.* **2019**, *86*, 410−419.
(40) Ali, G. M. E.; Ibrahim, D. A.; Elmetwali, A. M.; Ismail, N. S. M. Design, synthesis and biological evaluation of certain CDK2 inhibitors based on pyrazole and pyrazolo[1,5-a] pyrimidine scaffold with apoptotic activity. *Bioorg. Chem.* **2019**, *86*, 1−14.
(41) Luo, Z.; Wang, B.; Chen, Y.; Liu, H.; Shi, L. Novel CXCR4 inhibitor CPZ1344 inhibits the proliferation, migration and angiogenesis of glioblastoma. *Pathol. Oncol. Res.* **2020**, *26* (4), 2597−2604.
(42) Dai, J.; Zhang, J.; Fu, D.; Liu, M.; Zhang, H.; Tang, S.; Wang, L.; Xu, S.; Zhu, W.; Tang, Q.; Zheng, P.; Chen, T. Design, synthesis and biological evaluation of 4-(4-aminophenoxy)picolinamide derivatives as potential antitumor agents. *Eur. J. Med. Chem.* **2023**, *257*, 115499−115512.
(43) Khan, T. M.; Gul, N. S.; Lu, X.; Kumar, R.; Choudhary, M. I.; Liang, H.; Chen, Z. F. Rhodium(III) complexes with isoquinoline derivatives as potential anticancer agents: in vitro and in vivo activity studies. *Dalton Trans.* **2019**, *48* (30), 11469−11479.
(44) Lord, R. M.; Zegke, M.; Basri, A. M.; Pask, C. M.; McGowan, P. C. Rhodium(III) dihalido complexes: The effect of ligand substitution and halido coordination on increasing cancer cell potency. *Inorg. Chem.* **2021**, *60* (3), 2076−2086.
(45) Almodares, Z.; Lucas, S. J.; Crossley, B. D.; Basri, A. M.; Pask, C. M.; Hebden, A. J.; Phillips, R. M.; McGowan, P. C. Rhodium, iridium, and ruthenium half-sandwich picolinamide complexes as anticancer agents. *Inorg. Chem.* **2014**, *53* (2), 727−736.
(46) Gu, Y. Q.; Shen, W. Y.; Zhou, Y.; Chen, S. F.; Mi, Y.; Long, B. F.; Young, D. J.; Hu, F. L. A pyrazolopyrimidine based fluorescent probe for the detection of Cu(2+) and Ni(2+) and its application in living cells. *Spectrochim. Acta, Part A* **2019**, *209*, 141−149.
(47) Mak, S.-T.; Yam, V. W.-W.; Che, C.-M.; Mak, T. C. W. Synthesis, reactivities, and electrochemical properties of pyridinecarboxamide complexes of rhodium(III) and iridium(III). Crystal structure of $[Rh(bpb)(py)_2]ClO_4$[H_2bpb = 1,2-bis(2-pyridinecarboxamido)benzene, py = pyridine]. *J. Chem. Soc., Dalton Trans.* **1990**, *8*, 2555−2564.
(48) Ng, F. N.; Zhou, Z.; Yu, W. Y. [Rh(III)(Cp*)]-catalyzed ortho-selective direct C(sp(2))-H bond amidation/amination of benzoic acids by N-chlorocarbamates and N-chloromorpholines. A versatile synthesis of functionalized anthranilic acids. *Chemistry* **2014**, *20* (15), 4474−4480.
(49) Huang, H.; Zhang, P.; Chen, H.; Ji, L.; Chao, H. Comparison between polypyridyl and cyclometalated ruthenium(II) complexes: Anticancer activities against 2D and 3D cancer models. *Chemistry* **2015**, *21* (2), 715−725.
(50) Guo, L.; Hu, X.; Yang, Y.; An, W.; Gao, J.; Liu, Q.; Liu, Z. Synthesis and biological evaluation of zwitterionic half-sandwich rhodium(III) and ruthenium(II) organometallic complexes. *Bioorg. Chem.* **2021**, *116*, 105311−105321.
(51) Kordestani, N.; Amiri Rudbari, H.; Fernandes, A. R.; Raposo, L. R.; Luz, A.; Baptista, P. V.; Bruno, G.; Scopelliti, R.; Fateminia, Z.; Micale, N.; Tumamov, N.; Wouters, J.; Kajani, A. A.; Bordbar, A. K. Copper(II) complexes with tridentate halogen-substituted Schiff base ligands: Synthesis, crystal structures and investigating the effect of halogenation, leaving groups and ligand flexibility on antiproliferative activities. *Dalton Trans.* **2021**, *50* (11), 3990−4007.
(52) Wang, M.; Lv, C. Y.; Li, S. A.; Wang, J. K.; Luo, W. Z.; Zhao, P. C.; Liu, X. Y.; Wang, Z. M.; Jiao, Y.; Sun, H. W.; Zhao, Y.; Zhang, P. Near infrared light fluorescence imaging-guided biomimetic nanoparticles of extracellular vesicles deliver indocyanine green and paclitaxel for hyperthermia combined with chemotherapy against glioma. *J. Nanobiotechnology* **2021**, *19* (1), 210−227.
(53) Hao, L.; Li, Z. W.; Zhang, D. Y.; He, L.; Liu, W.; Yang, J.; Tan, C. P.; Ji, L. N.; Mao, Z. W. Monitoring mitochondrial viscosity with anticancer phosphorescent Ir(III) complexes via two-photon lifetime imaging. *Chem. Sci.* **2019**, *10* (5), 1285−1293.
(54) Komor, A. C.; Barton, J. K. The path for metal complexes to a DNA target. *Chem. Commun.* **2013**, *49* (35), 3617−3630.
(55) Pandey, N.; Black, B. E. Rapid detection and signaling of DNA damage by PARP-1. *Trends Biochem. Sci.* **2021**, *46* (9), 744−757.
(56) Zhang, Z.; Yu, P.; Gou, Y.; Zhang, J.; Li, S.; Cai, M.; Sun, H.; Yang, F.; Liang, H. Novel brain-tumor-inhibiting copper(II) compound based on a human serum albumin (HSA)-cell penetrating peptide conjugate. *J. Med. Chem.* **2019**, *62* (23), 10630−10644.
(57) Yao, H.; Xie, S.; Ma, X.; Liu, J.; Wu, H.; Lin, A.; Yao, H.; Li, D.; Xu, S.; Yang, D. H.; Chen, Z. S.; Xu, J. Identification of a potent oridonin analogue for treatment of triple-negative breast cancer. *J. Med. Chem.* **2020**, *63* (15), 8157−8178.
(58) Gerle, C. Mitochondrial F-ATP synthase as the permeability transition pore. *Pharmacol. Res.* **2020**, *160*, 105081−105091.
(59) Huang, H.; Long, S.; Li, M.; Gao, F.; Du, J.; Fan, J.; Peng, X. Bromo-pentamethine as mitochondria-targeted photosensitizers for cancer cell apoptosis with high efficiency. *Dyes Pigm.* **2018**, *149*, 633−638.
(60) Jangili, P.; Kong, N.; Kim, J. H.; Zhou, J.; Liu, H.; Zhang, X.; Tao, W.; Kim, J. S. DNA-damage-response-targeting mitochondria-activated multifunctional prodrug strategy for self-defensive tumor therapy. *Angew. Chem., Int. Ed.* **2022**, *61* (16), No. e202117075.

https://doi.org/10.1021/acs.jmedchem.3c00318
J. Med. Chem. 2023, 66, 9592−9606

(61) Shang, Y.; Xue, W.; Kong, J.; Chen, Y.; Qiu, X.; An, X.; Li, Y.; Wang, H.; An, J. Ultrafine black carbon caused mitochondrial oxidative stress, mitochondrial dysfunction and mitophagy in SH-SY5Y cells. *Sci. Total Environ.* **2022**, *813*, 151899−151908.
(62) Naryzhnaya, N. V.; Maslov, L. N.; Oeltgen, P. R. Pharmacology of mitochondrial permeability transition pore inhibitors. *Drug Dev. Res.* **2019**, *80* (8), 1013−1030.
(63) Wang, P.; Gong, Q.; Hu, J.; Li, X.; Zhang, X. Reactive oxygen species (ROS)-responsive prodrugs, probes, and theranostic prodrugs: Applications in the ROS-related diseases. *J. Med. Chem.* **2021**, *64* (1), 298−325.
(64) Daks, A.; Shuvalov, O.; Fedorova, O.; Parfenyev, S.; Simon, H. U.; Barlev, N. A. Methyltransferase Set7/9 as a multifaceted regulator of ROS response. *Int. J. Biol. Sci.* **2023**, *19* (8), 2304−2318.
(65) Wang, K.; Zhu, C.; He, Y.; Zhang, Z.; Zhou, W.; Muhammad, N.; Guo, Y.; Wang, X.; Guo, Z. Restraining cancer cells by dual metabolic inhibition with a mitochondrion-targeted platinum(II) complex. *Angew. Chem., Int. Ed.* **2019**, *58* (14), 4638−4643.
(66) Hassan, A. H. E.; Wang, C. Y.; Lee, H. J.; Jung, S. J.; Kim, Y. J.; Cho, S. B.; Lee, C. H.; Ham, G.; Oh, T.; Lee, S. K.; Lee, Y. S. Scaffold hopping of N-benzyl-3,4,5-trimethoxyaniline: 5,6,7-Trimethoxyflavan derivatives as novel potential anticancer agents modulating hippo signaling pathway. *Eur. J. Med. Chem.* **2023**, *256*, 115421−115432.
(67) Denis, C.; Sopkova-de Oliveira Santos, J.; Bureau, R.; Voisin-Chiret, A. S. Hot-spots of Mcl-1 protein. *J. Med. Chem.* **2020**, *63* (3), 928−943.
(68) Li, H.; Fan, T. J.; Zou, P.; Xu, B. Diclofenac sodium triggers p53-dependent apoptosis in human corneal epithelial cells via ROS-mediated crosstalk. *Chem. Res. Toxicol.* **2021**, *34* (1), 70−79.
(69) Meza-Sosa, K. F.; Miao, R.; Navarro, F.; Zhang, Z.; Zhang, Y.; Hu, J. J.; Hartford, C. C. R.; Li, X. L.; Pedraza-Alva, G.; Perez-Martinez, L.; Lal, A.; Wu, H.; Lieberman, J. SPARCLE, a p53-induced lncRNA, controls apoptosis after genotoxic stress by promoting PARP-1 cleavage. *Mol. Cell* **2022**, *82* (4), 785−802.e10.
(70) Zhong, L.; Xia, Y.; He, T.; Wenjie, S.; Jinxia, A.; Lijun, Y.; Hui, G. Polymeric photothermal nanoplatform with the inhibition of aquaporin 3 for anti-metastasis therapy of breast cancer. *Acta Biomater.* **2022**, *153*, 505−517.
(71) Zhang, S.; Yang, G.; Guan, W.; Li, B.; Feng, X.; Fan, H. Autophagy plays a protective role in sodium hydrosulfide-induced acute lung injury by attenuating oxidative stress and inflammation in rats. *Chem. Res. Toxicol.* **2021**, *34* (3), 857−864.
(72) Li, D.; Wang, H.; Ding, Y.; Zhang, Z.; Zheng, Z.; Dong, J.; Kim, H.; Meng, X.; Zhou, Q.; Zhou, J.; Fang, L. Targeting the NRF-2/RHOA/ROCK signaling pathway with a novel aziridonin, YD0514, to suppress breast cancer progression and lung metastasis. *Cancer Lett.* **2018**, *424*, 97−108.
(73) Kim, J. H.; Ofori, S.; Parkin, S.; Vekaria, H.; Sullivan, P. G.; Awuah, S. G. Anticancer gold(III)-bisphosphine complex alters the mitochondrial electron transport chain to induce in vivo tumor inhibition. *Chem. Sci.* **2021**, *12* (21), 7467−7479.
(74) Nurmamat, M.; Yan, H.; Wang, R.; Zhao, H.; Li, Y.; Wang, X.; Nurmaimaiti, K.; Kurmanjiang, T.; Luo, D.; Baodi, J.; Xu, G.; Li, J. Novel copper(II) complex with a 4-Acylpyrazolone derivative and coligand induce apoptosis in liver cancer cells. *ACS Med. Chem. Lett.* **2021**, *12* (3), 467−476.
(75) Schoepfer, J.; Jahnke, W.; Berellini, G.; Buonamici, S.; Cotesta, S.; Cowan-Jacob, S. W.; Dodd, S.; Drueckes, P.; Fabbro, D.; Gabriel, T.; Groell, J.; Grotzfeld, R. M.; Hassan, A. Q.; Henry, C.; Iyer, V.; Jones, D.; Lombardo, F.; Loo, A.; Manley, P. W.; Pellé, X.; Rummel, G.; Salem, B.; Warmuth, M.; Wylie, A. A.; Zoller, T.; Marzinzik, A. L.; Furet, P. Discovery of Asciminib (ABL001), an Allosteric Inhibitor of the Tyrosine Kinase Activity of BCR-ABL1. *J. Med. Chem.* **2018**, *61* (18), 8120−8135.

https://doi.org/10.1021/acs.jmedchem.3c00318
J. Med. Chem. 2023, 66, 9592−9606